Analysis of quality, aggregation and toxicity of amyloid beta peptide produced by JPT

Annelies Vandersteen[1,2,*], Ellen Hubin[1,2,*], Greet De Baets[1], Kerensa Broersen[1,2]

[1]Free University of Brussels (VUB), Brussels, Belgium
[2]University of Twente, Enschede, The Netherlands
[*]Equal contribution

28 June 2011

Aim

To evaluate the quality, aggregation behaviour and toxic impact of a variety of amyloid beta peptide variants produced by JPT.

Selection of peptides

Peptides were rationally selected for this study and included:

- *Wild type Aβ1-37, Aβ1-38, Aβ1-40, Aβ1-42, Aβ1-43.* These peptides represent the range of naturally present Aβ peptide lengths in the brains of healthy and diseased subjects as a result of variable γ-secretase induced cleavage of the Amyloid Precursor Protein (APP). Patients suffering from Alzheimer's disease often produce the longer forms of Aβ (Aβ1-42, Aβ1-43) while healthy subjects produce more of the shorter Aβ1-37, Aβ1-38 and Aβ1-40. (Younkin 1998, Wiltfang et al 2002, Lewczuk et al 2003, Maddalena et al 2004).

- *P3 peptides Aβ17-40 and Aβ17-42.* Aβ is produced by sequential processing of APP by β- and γ-secretases, also termed the 'amyloidogenic pathway'. Alternatively APP can be processed into so-called p3 peptides by sequential cleavage mediated by α- and γ-secretases. This pathway is called 'non amyloidogenic' (Fig. 1). It is not clear which mechanisms are responsible for selection of either the p3 or Aβ-producing pathway, although shifts in the lipid composition of the membrane have been proposed to regulate recruitment of either the α- or β-secretase to mediate APP cleavage (Abad-Rodriguez et al 2004).

- C-terminally and N-terminally biotinylated forms of Aβ1-40 and Aβ1-42. Biotinylated forms of Aβ are regularly used for interaction studies (Nelson and Alkon 2007, Bohrmann et al 1999, Liu et al 2005, Leissring et al 2003). Initially the C-terminal region was recognized as the primary aggregation-inducing segment of Aβ, further

supported by the finding that the longer Aβ1-42 is more aggregation-prone than the shorter Aβ1-40 (Snyder et al 1994, Frost et al 2003, Yoshiike et al 2003, Wang et al 2006, Kim et al 2007, Yan and Wang 2007, Jan et al 2008). Recently it has been recognized that also the N-terminal region may play a role in regulating the aggregation properties of Aβ (Brorsson et al 2010) raising the experimental requirement for both C- and N-terminally biotinylated forms of the peptide.

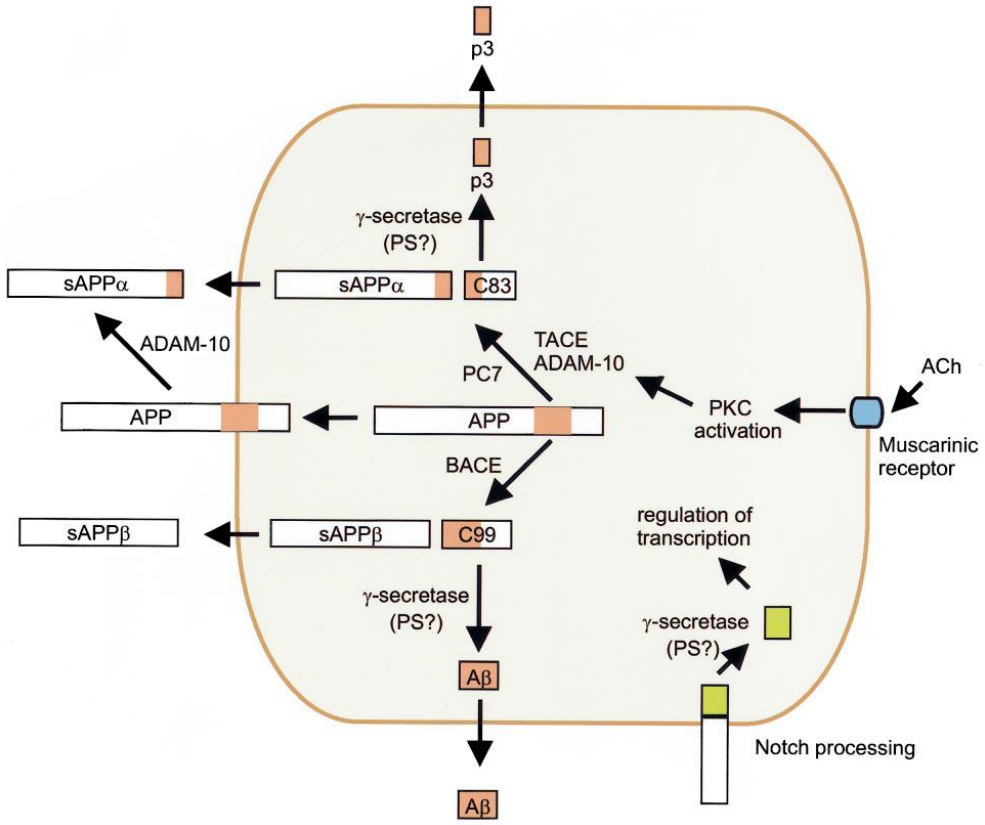

Figure 1 Pathways of APP processing by α-, β- and γ-secretases. Cleavage by α-secretase (PC7, TACE or ADAM-10) produces sAPPα and a C-terminal fragment C83. Both TACE and ADAM-10 can be activated by protein kinase C (PKC) which is regulated by the muscarinic acetylcholine (ACh) receptor. C83 is cleaved by γ-secretase to produce p3. Cleavage of APP by β-secretase (BACE) produces sAPPβ and C99. γ-Secretase, also believed to play a role in the proteolysis of Notch, cleaves C99 to release Aβ which has neurotoxic properties. Presenilins (PS) 1 and 2 have been proposed as γ-secretases (image and legend obtained from Nunan and Small 2000).

- Familial Alzheimer's disease related missense mutations. A number of mutations have been identified in the sequence of Aβ1-42 which are related to familial cases of Alzheimer's disease. These mutations include:
    - D7N, the Tottori mutation (Wakutani et al 2004).
    - E11K, the Leuven mutation (Zhou et al 2011).

- A21G, the Flemish mutation (Hendriks et al 1992).
- E22G, the Arctic mutation (Kamino et al 1992).
- E22Q, the Dutch mutation (Levy et al 1990).
- E22K, the Italian mutation (Bugiani et al 2010).
- D23N, the Iowa mutation (Grabowski et al 2001).

Materials

Beta-amyloid (1-43) (batch no. 231210_Aβ-1-43), beta-amyloid (1-42) (batch no. 231210_Aβ-1-42), Asp7Asn-beta-amyloid (1-42) (batch no. 080211_D7N-Aβ-1-42), Glu11Lys-Aβ 1-42 (batch no. 231210_E11K-Aβ-1-42), Glu22Gly Aβ 1-42 (batch no. 231210_E22G-Aβ-1-42), Ala21Gly Aβ 1-42 (batch no. 231210_A21G-Aβ-1-42), Glu22Lys-Aβ 1-42 (batch no. 090211_E22K-Aβ-1-42), Glu22Gln-Aβ 1-42 (batch no. 090211_E22Q-Aβ-1-42), Asp23Asn-Aβ 1-42 (batch no. 090211_D23N-Aβ-1-42), Aβ 1-42-Lys(Biotinoyl) (batch no. 090211_Aβ-1-42-Lys(Biot)), Biotinoyl-Aβ 1-42 (batch no. 231210_Biot.-Aβ-1-42), Aβ 1-40 (batch no. 231210_Aβ-1-40), Biotinoyl-Aβ 1-40 (batch no. 231210_Biot.-Aβ-1-40), Aβ 1-40-Lys(Biotinoyl) (batch no. 090211_Aβ-1-40-Lys(Biot)), Aβ 1-37 (batch no. 060211_Aβ-1-37), Aβ 1-38 (batch no. 060211_Aβ-1-38), Aβ 17-40 (batch no. 090211_Aβ-17-40), and Aβ 17-42 (batch no. 090211_Aβ-17-42), all produced by JPT.

Methods

In silico prediction of aggregation

The statistical mechanics algorithm Tango was used to predict aggregation-prone regions in the Aβ peptide (Fernandez-Escamilla et al. 2004). Tango provides an aggregation propensity (0–100%) per residue as output. An aggregating region is defined as a continuous stretch of residues with a Tango score higher than 0% and a total score higher than 50%. Tango calculations were performed via http://tango.switchlab.org/ at a pH of 7.0, a temperature of 298.15 K and 0.02 M ionic strength without N- or C- terminal protection. The Waltz algorithm is a binary predictor designating amyloid-forming regions in a given sequence (Maurer-Stroh et al. 2010). Calculations were performed via http://waltz.switchlab.org/ at pH 7.0 using either high specificity (showed as 100%) or high sensitivity (showed as 25%) threshold. These algorithms cannot take into account modification of the peptide through biotinylation, hence we included in the calculations only the addition of the extra lysine for Aβ-K-biot samples.

Dissolving peptides

Peptides were dissolved according to the standard procedure developed and validated in our laboratory (Broersen et al. 2011). Aβ peptides were dissolved at a concentration of 1 mg/mL in hexafluoroisopropanol (HFIP) (99%, Aldrich Cat. # 10,522-8). The HFIP was evaporated

using a gentle stream of nitrogen gas and the peptide film was resolved using dimethyl sulfoxide (DMSO), (Sigma Cat. # D4540) to a final peptide concentration of 1 mg/mL. The peptide was separated from DMSO by elution using a 5 mL HiTrap™ desalting column (GE Healthcare, Sweden) and the resulting sample was collected in two fractions of 500 μL. Complete removal of DMSO was confirmed by FTIR: DMSO provides spectral maxima at 1011 and 951 cm^{-1}. The peptide was eluted into a 50 mM Tris, 1 mM EDTA buffer, pH 7.5 and the peptide concentration was measured using Bradford assay. The samples were kept on ice until experiments started, with a maximum lag time of 30 min.

Yield

Assuming that each vial contained precisely 0.5 mg material the maximum concentration of Aβ obtained in 1 mL upon dissolving should be 110 μM (mW of Aβ is 4.4 kDa). The concentration of Aβ upon solubilization according to above procedure was determined using the Bradford assay. The yield was calculated according to below equation:

$$\text{Yield (\%)} = \frac{\text{Aβ concentration determined in solution}}{110\ \mu\text{M}} * 100$$

Solubility

The Aβ solutions were centrifuged at maximum speed in a tabletop centrifuge for 1 min to sediment material which had not been fully dissolved. The concentration of Aβ in the supernatant was determined using the Bradford assay. Measurements were performed in triplicate on three different Aβ preparations. The solubility was calculated according to below equation:

$$\text{Solubility (\%)} = \frac{\text{concentration Aβ in supernatant}}{\text{total Aβ concentration}} * 100$$

Thioflavin T fluorescence

Aβ was diluted to a concentration of 1 μM in the presence of a final concentration of 12 μM Thioflavin T and 50 mM Tris, 1 mM EDTA, pH 7.4. The fibrillization kinetics of the various Aβ preparations were monitored *in situ* using a Fluostar OPTIMA fluorescence plate reader at an excitation wavelength of 440 nm and an emission wavelength of 480 nm. Fluorescence readings were recorded every 5 min for a period of 20 h. Measurements were performed as three independent triplicates. Recorded values were averaged and background measurements were subtracted including buffer containing 12 μM Thioflavin T.

Cytotoxicity

Cytotoxicity of Aβ was monitored using the CellTiter Blue reagent (Promega) which is a buffered solution containing the dye resazurin. Viable cells take up dark-blue non-fluorescent resazurin and convert it into bright-pink highly fluorescent resorufin. The eluted

Aβ preparations were normalized to a concentration of 50 μM using 50 mM Tris, 1 mM EDTA, pH 7.4. Samples were incubated at 25°C for 1.5 h. After incubation the Aβ solutions were diluted to 5 μM in DMEM:F12 and added to neuroblastoma SHSY-5Y cells which had grown at 22,000 cells/well in a 96-well plate for 24 to 48 h. After another 24 h incubation at 37°C, 5% CO_2 in the presence of Aβ, 10 μL CellTiter Blue reagent (Promega) was added to each well and incubated for 4 h. The fluorescence intensity was determined at an excitation wavelength of 544 nm and an emission wavelength of 590 nm. Controls included 50 mM Tris, 1 mM EDTA buffer, and staurosporine at a final concentration of 1 μM. Measurements were performed as three independent replicates.

Transmission Electron Microscopy

After 2 weeks incubation at 25°C, 5 μL sample was incubated on top of a carbon-coated Formvar 400 mesh grid (Agar Scientific) for 1 min. Excess solution was removed by blotting. The grid was washed in a 50 μL drop of filtered Ultrapure water (Merck) and subsequently stained in a 50 μL drop of 1% uranyl acetate followed by blotting off excess solution. Samples were examined using a Jeol JEM-1400 TEM at an accelerating voltage of 80 kV and images were digitalized using a CCD camera. Images were collected of three independently prepared Aβ preparations.

Dotblot

Upon elution of Aβ from the column and after 2 weeks of incubation at 25°C, a volume of 5 μL sample was spotted on a nitrocellulose membrane (Protran BA85, Whatman). The membranes were blocked at 25 °C in phosphate buffered saline containing 0.2% Tween for 1 h and incubated for 1 h at 25°C with primary A11 antibody, diluted 1:4000 in 100 mM Hepes, pH 7.0. After incubation with a secondary anti-rabbit-HRP-tagged antibody, diluted 1:5000 in phosphate buffered solution containing 0.05% Tween for 0.5 h at 25°C, the membranes were visualized using the Immobilon$_{TM}$ Western chemiluminescent HRP substrate system (Millipore, USA, Cat.# WBKLS0100).

Far-UV circular dichroism

Samples were incubated for 2 weeks at 25°C followed by dilution of Aβ to a concentration of 20 μM. Samples were placed in a quartz cuvette with a optical path of 1 mm and far-UV circular dichroism spectra were recorded in the wavelength range from 260 to 190 nm with 0.2 nm resolution, 2.0 sec response time, 2.0 nm bandwidth at a scanning speed of 50 nm/min. Data were collected as averages of eight scans. The spectra obtained were corrected by subtracting the spectrum obtained for buffer only. Spectra were analyzed for secondary structure elements using the CDSSTR analysis program supported by the Dichroweb website (http://dichroweb.cryst.bbk.ac.uk/html/home.shtml) developed by Birkbeck College at the University of London (UK).

Results

In silico prediction of aggregation

Using the Tango and Waltz algorithms which have been developed by the Switch laboratory at the Free University of Brussels (VUB) we aimed to obtain a preliminary impression of the changes in aggregation parameters which can be expected upon mutation of the Aβ peptide. We first compared the Waltz and Tango scores of the Aβ peptides varying in length from 37 to 43 amino acids in length (Fig. 2).

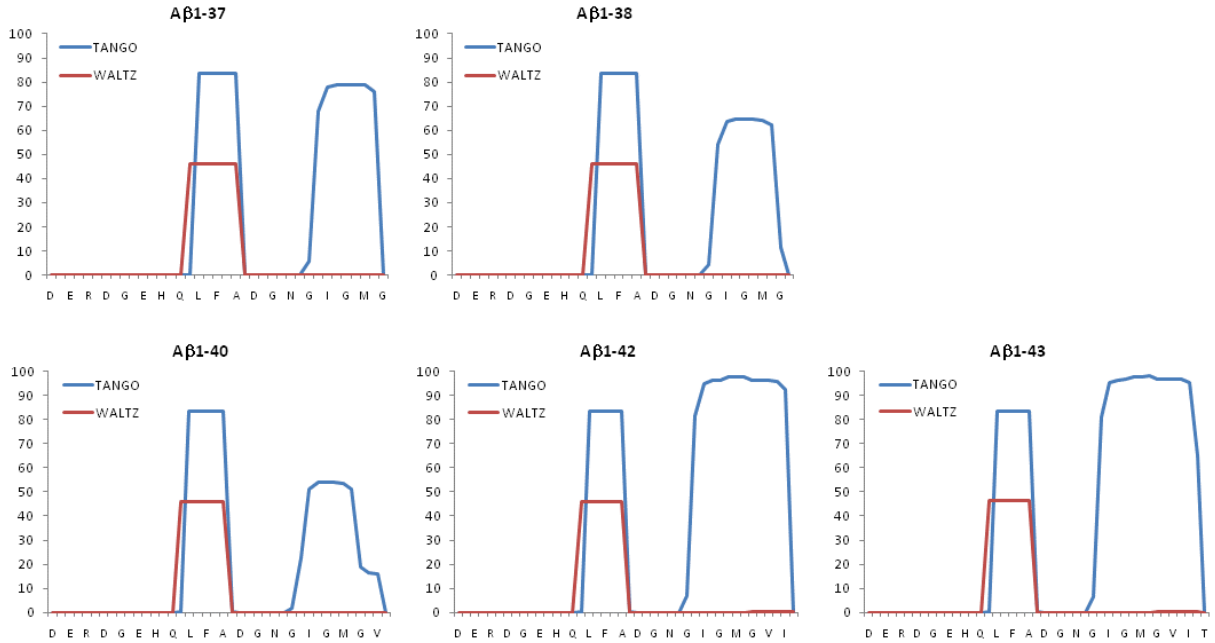

Figure 2 Aggregation propensities predicted by Tango and Waltz for Aβ peptides varying in length. The blue line denotes the Tango score and the red line the Waltz score. The y-axis presents the aggregation propensity calculated for each algorithm. The x-axis shows the primary sequence of Aβ.

Figure 2 shows that Aβ has two distinct Tango (blue) zones, the first zone is located in the central region of the peptide and the intensity of this region does not change with variation of the Aβ peptide length. The second zone is located in the C-terminal region and shows strong variation with peptide length although not in a linear fashion: for Aβ42 and Aβ43 the C-terminal zone dominantly determines the aggregation of the Aβ peptide while the intensity of the central region suggests that this stretch more importantly determines the aggregation behavior of Aβ37, Aβ38 and Aβ40. The five peptides all show one distinct Waltz (red) region located in the central region of the peptide, which does not vary with peptide length.

The two p3 peptides Aβ17-40 and Aβ17-42 both show a single positive Tango region and no Waltz region. The removal of the N-terminal 16 amino acids eliminated the central Tango region completely. The two additional C-terminal amino acids of Aβ17-42 induce a larger Tango intensity compared to Aβ17-40 (Fig. 3).

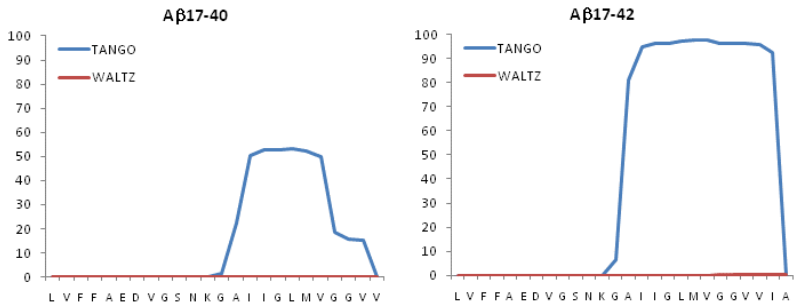

Figure 3 Aggregation propensities predicted by Tango and Waltz for p3 peptides. The blue line denotes the Tango score and the red line the Waltz score. The y-axis presents the aggregation propensity calculated for each algorithm. The x-axis shows the primary sequence of Aβ.

Figure 4 shows the effect of lysine addition to aid biotinylation on the predicted aggregation propensities of Aβ40 and Aβ42. As both Tango and Waltz cannot take modifications such as biotinylation into account the resulting Tango and Waltz scores are assumed to be similar to the unmodified peptides. The addition of a lysine on Aβ40 shows a strong inducing effect on the aggregation propensity calculated by the Tango algorithm, but not for the Waltz algorithm. Aβ42 is unaffected by this addition.

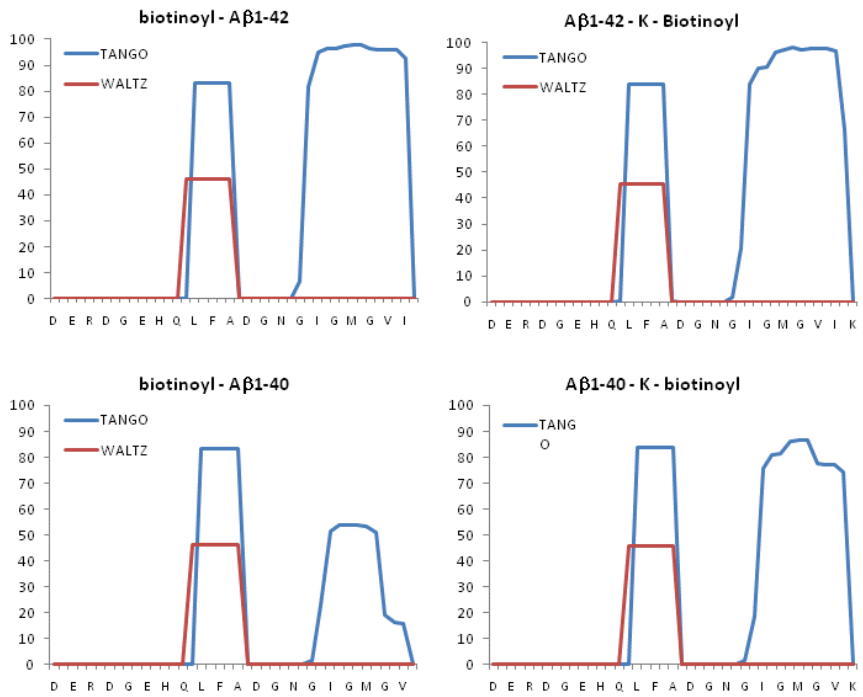

Figure 4 Aggregation propensities predicted by Tango and Waltz for biotinylated Aβ peptides. The blue line denotes the Tango score and the red line the Waltz score. The y-axis presents the aggregation propensity calculated for each algorithm. The x-axis shows the primary sequence of Aβ.

Seven Alzheimer's disease-related mutations have been reported: the Flemish mutation (Ala21 to Gly), Dutch mutation (Glu22 to Gln), Italian mutation (Glu22 to Lys), Arctic mutation (Glu22 to Gly), Iowa mutation (Asp23 to Asn), the Tottori mutation (Asp7 to Asn) Tottori, and recently our group identified a new mutation Glu11 to Lys. All mutations occur either in the N-terminal region (D7N, E11K) or in the central region of the peptide (A21G, E22G, E22K, E22Q, D23N) and are therefore expected to affect the predicted aggregation propensity of Aβ. The C-terminal Tango region is not affected and no second Waltz region is induced by any of the mutations (Fig. 5). The central region of Aβ is affected by the mutations as can be expected by their location. Mutations D7N, E11K, and E22K have no effect, A21G strongly inhibits while E22G, E22Q and D23N enhance the Tango predicted aggregation propensity of Aβ42. Mutations D7N, E11K and E22K also show no effect on the Waltz score but A21G, E22G, E22Q and D23N inhibit the Waltz score of the Waltz region.

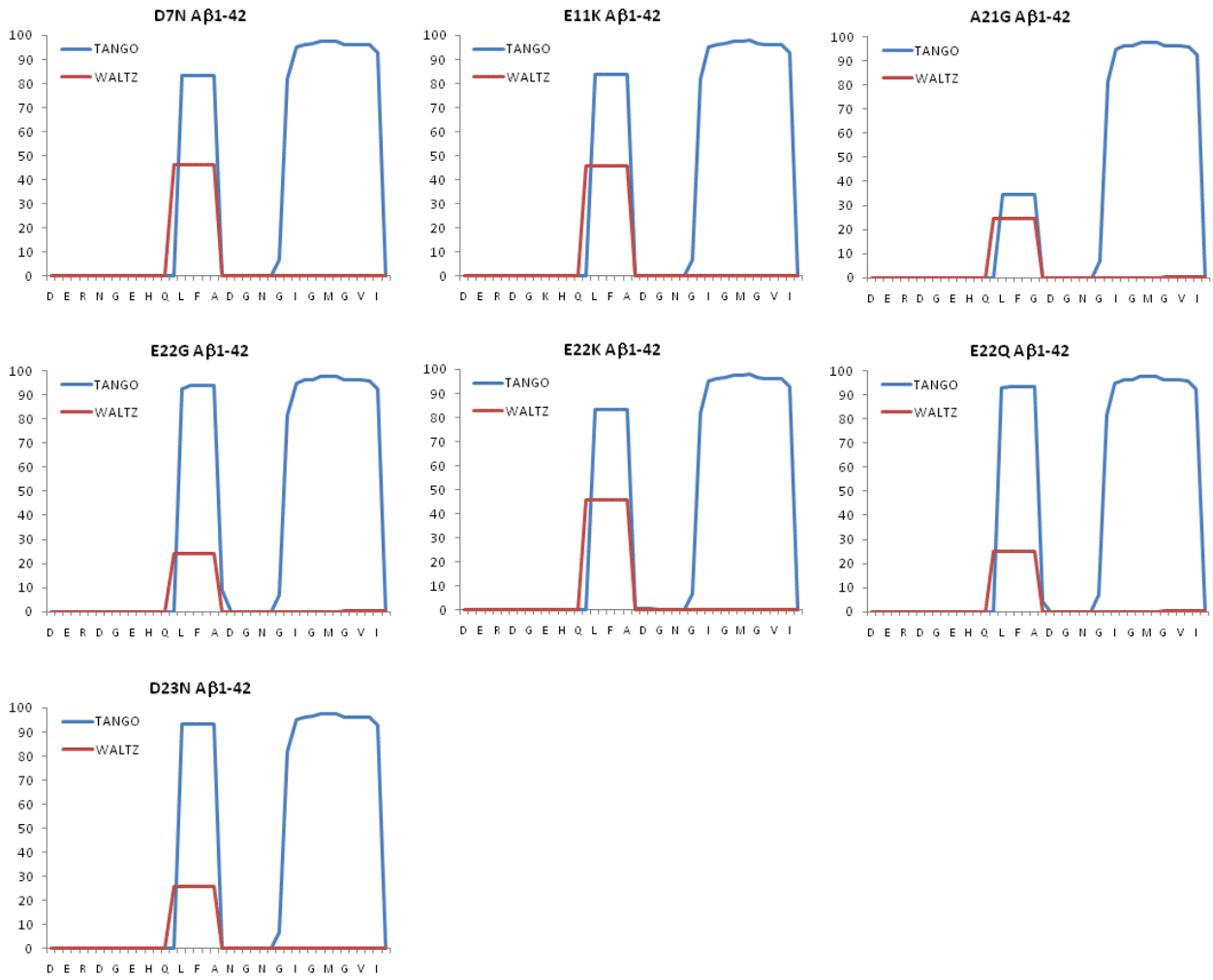

Figure 5 Aggregation propensities predicted by Tango and Waltz for Alzheimer's disease-related Aβ mutations. The blue line denotes the Tango score and the red line the Waltz score. The y-axis presents the aggregation propensity calculated for each algorithm. The x-axis shows the primary sequence of Aβ.

Figure 6 shows the total Tango and Waltz scores for all Aβ preparations. Wild type aggregating Aβ42 has a Tango score of 1564 while Aβ40 (which is not aggregation-prone) has a Tango score of 810. Aβ37 and Aβ38 have slightly higher Tango scores than Aβ40 with 961 and 872, respectively, suggesting that shorter Aβ peptides are not necessarily predicted to have lower propensity to aggregate. As preliminary *in vitro* experiments in our laboratory also show, shorter Aβ peptides are indeed not less aggregation prone than Aβ40. Truncated p3 peptides have Tango scores of 385 and 1145 for Aβ17-40 and Aβ17-42, respectively. Even though the central aggregating region remains intact for these two peptides, clearly the N-terminal region plays an inducing role. The addition of a lysine in the biotinylated Aβ40 increases the Tango score from 810 for wild type Aβ40 to 1243 for Aβ40 containing a C-terminal lysine and thus potentially importantly affects the aggregation propensity of this

peptide. Aβ42 is not affected by the addition of a C-terminal lysine (Tango score 1551). Known disease-related mutations in the Aβ42 peptide sometimes marginally increase (E22G: 1623, E22Q: 1617, D23N 1613), inhibit (A21G: 1320) or maintain a similar Tango score (D7N: 1564, E11K: 1566, E22K: 1567) compared to wild type Aβ42.

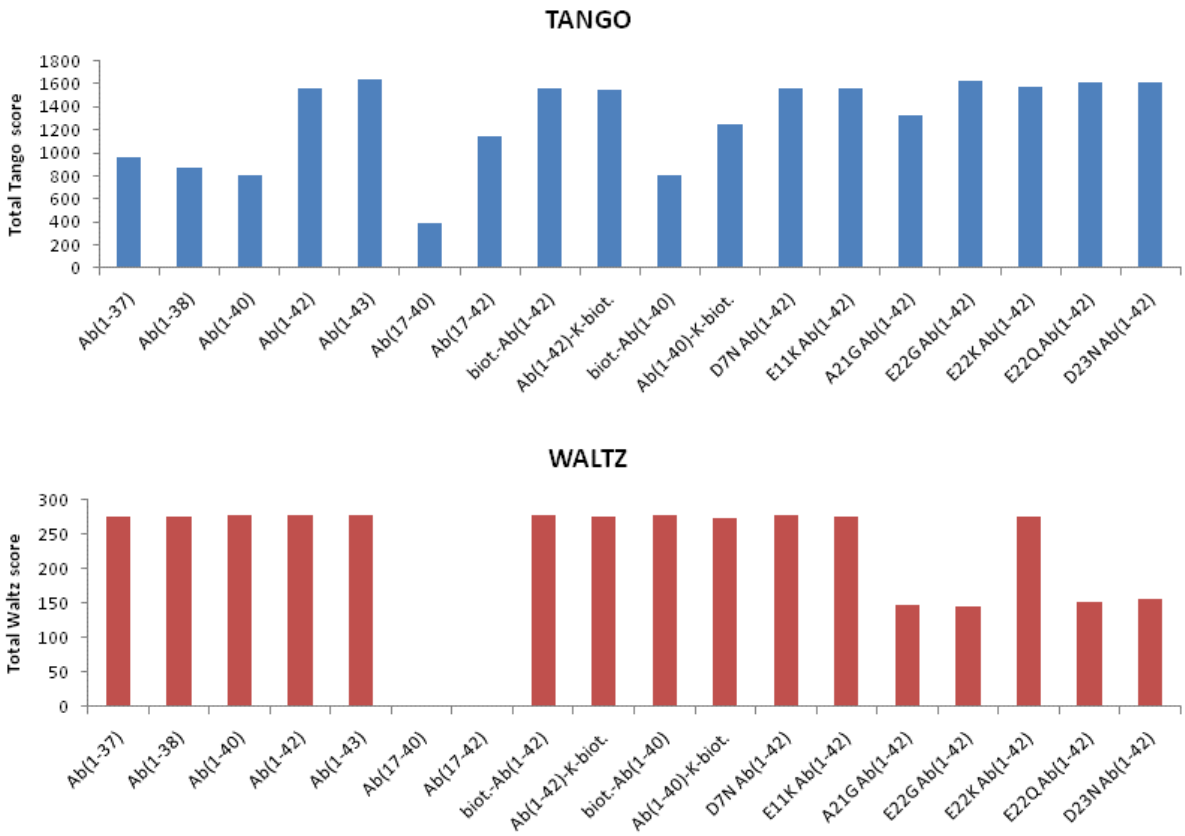

Figure 6 Total Waltz and Tango scores for each individual peptide.

The Waltz score is not affected by many of the mutations or truncations introduced but the p3 peptides both result in deletion of the Waltz region. Disease-related mutations A21G, E22G, E22Q and D23N all cause a significant (~ 50%) reduction in Waltz scores.

Yield

Assuming that each vial contained precisely 0.5 mg material the maximum concentration of Aβ obtained in 1 mL upon dissolving should be 110 μM. The concentration of Aβ in the solution was determined using absorption upon addition of Bradford reagent. In below figure 7 the determined Aβ concentration in the solution is expressed as a percentage of the theoretical concentration of 110 μM, called the yield.

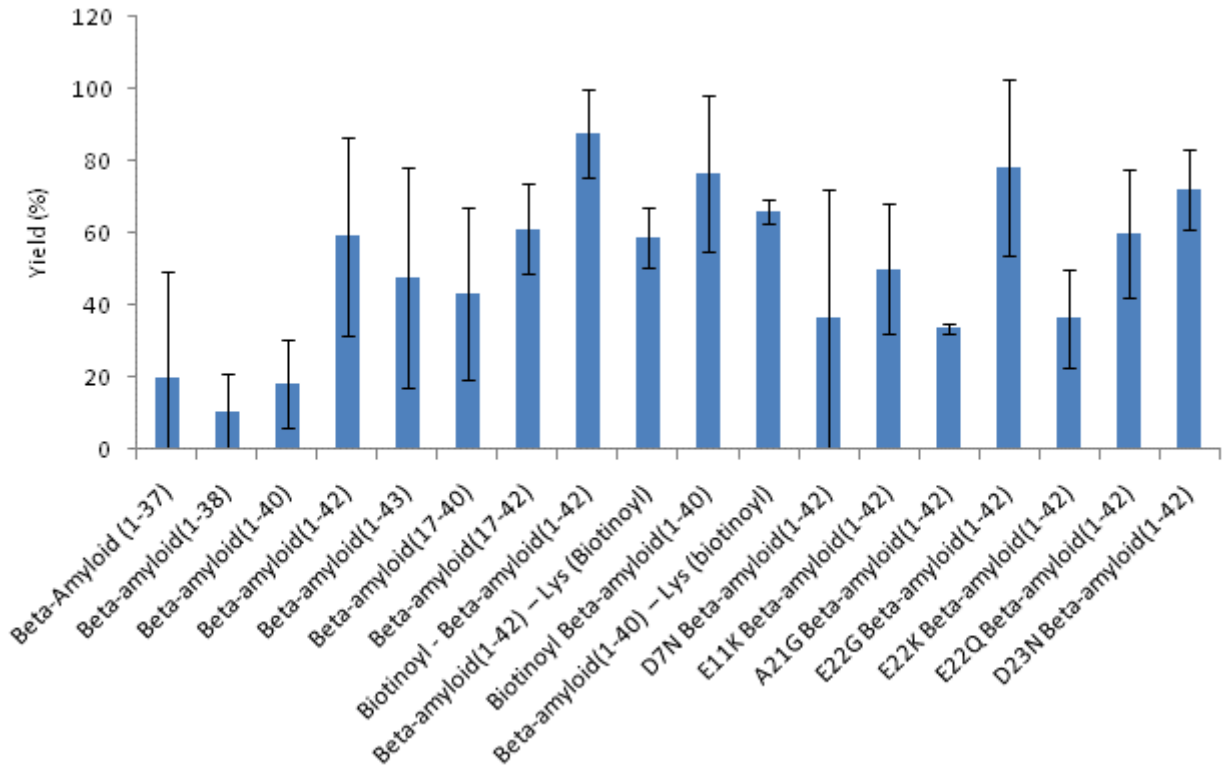

Figure 7 Yield of Aβ peptides upon dissolving. The error bars represent standard deviations.

Some peptides are well soluble. A yield of 70% or more of the theoretically expected Aβ concentration was detected in the final solutions of these peptides which include biotinylated Aβ42, biotinylated Aβ40, E22G Aβ42 and D23N Aβ42. The yield is not linked directly with the calculated Waltz or Tango scores: *i.e.* expected aggregation-prone peptides such as E22G Aβ42 and little aggregation-prone biotinylated Aβ40 both have a reasonable yield. Peptides with less than 25% yield include Aβ37 (20%), Aβ38 (11%) and Aβ40 (18%).

Further noticeable is the low reproducibility of the yield for some peptides, which include D7N Aβ42, Aβ17-40, Aβ43, Aβ42 and Aβ37. This assay was based on the assumption that each vial contained precisely 0.5 mg Aβ peptide. Further, the Bradford reagent used for this assay may differentially bind to more or less aggregated forms of the peptide, affecting reproducibility.

<u>Solubility</u>

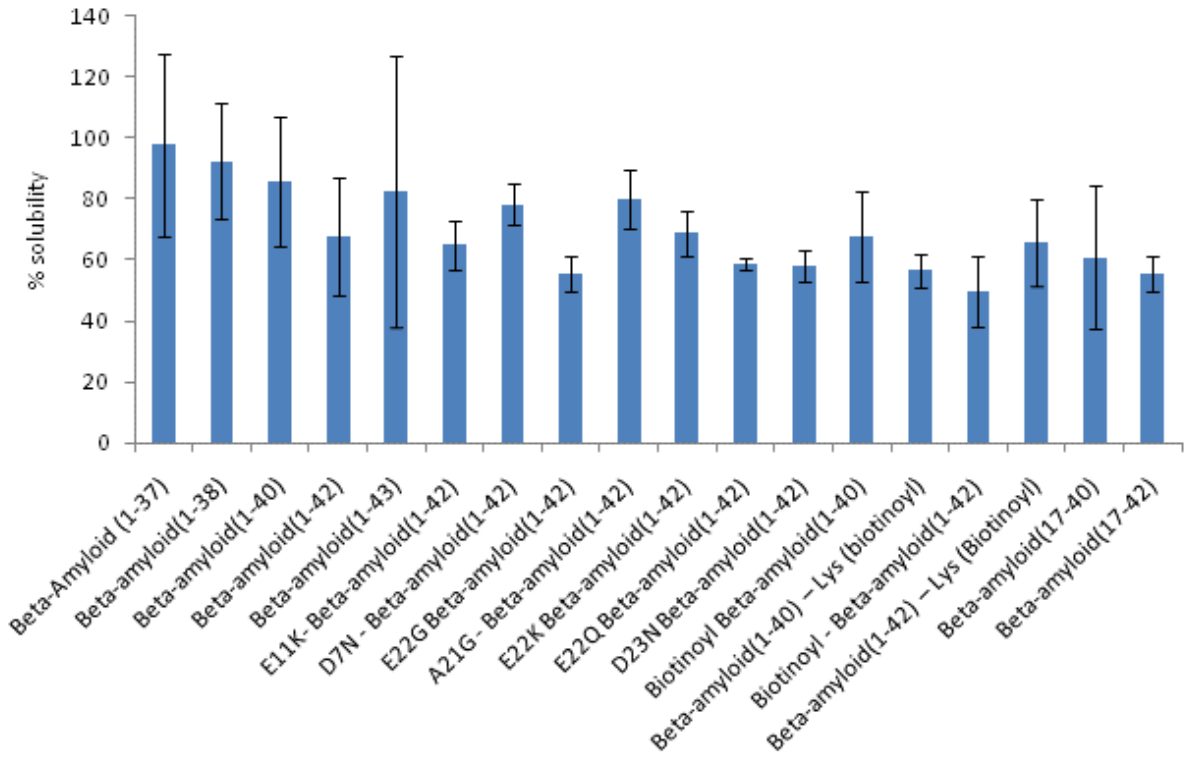

Figure 8 Solubility of Aβ peptides. The error bars represent standard deviations.

Once eluted off the column, the crude solubility of the peptides was tested by centrifugation of remaining undissolved material and determination of the concentration of peptide in the supernatant, which will primarily contain monomeric or small oligomeric Aβ. Most peptides were retained 50% or more in the supernatant with lowest solubility for biotinoyl-Aβ42 (49%). Highest solubility was found for Aβ37 and Aβ38 which retained 98% and 92% of the material in soluble form, respectively (Fig. 8).

Secondary structure determination by Far-UV Circular Dichroism

Upon incubation for 2 weeks we examined the secondary structure of the Amyloid beta peptides using far-UV Circular Dichroism (CD). At wavelengths in the 'far UV' region from 190 to 250 nm the primary chromophore is the peptide bond. Secondary structure elements (α-helix, β-sheet, β-turn and random coil) can be extracted from the spectrum as each provides a unique and characteristic fingerprint spectrum (Fig. 9). Figure 9 shows typical spectra for α-helix (two minima at 228 and 208 nm, crosses through '0' ellipticity around 200 nm), β-sheet (one single minimum around 218 nm, crosses through '0' ellipiticity around 200 nm), and random coil (single minimum around 200 nm). As proteins are generally not composed of one single type of secondary structure, the derived spectra are complex and require analysis using specifically designed algorithms.

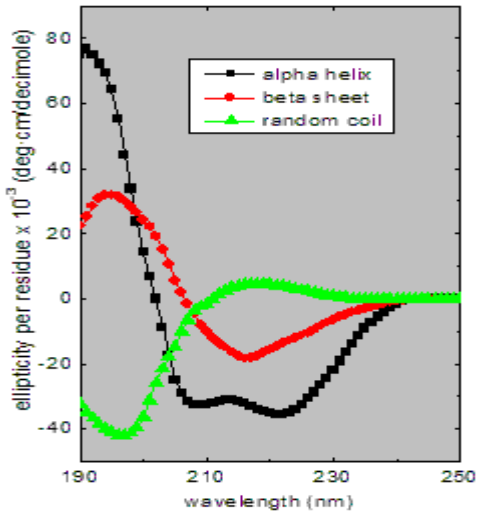

Figure 9 Fingerprint spectra for α-helix, β-sheet and random coil structure (source: http://www.ap-lab.com/circular_dichroism.htm).

Figure 10 shows the far-UV CD spectra for the different amyloid-beta peptide lengths 37, 38, 40, 42 and 43 upon incubation for 2 weeks. Aβ42 and Aβ43 show a clear signature for a predominantly β-sheet organized structure, which is characteristic for an aggregated protein. On the other hand, the spectra for Aβ37, Aβ38 and Aβ40 show a mixture of β-sheet aggregates, α-helical and disordered structure. Table 1 shows the values obtained after deconvolution of the spectra using the CDSSTR algorithm on the Dichroweb website (Lobley *et al.* 2002, Whitmore and Wallace 2008, Whitmore and Wallace 2004). The spectra of Aβ42 and Aβ43 are representative of 5-6% α-helix, >40% β-sheet and 31% random coil structure. The spectra for Aβ 37, Aβ38 and Aβ40 show 15-20% α-helix, 26-30% β-sheet, and a variation in random coil content of 27%, 42% and 30% for Aβ37, Aβ38 and Aβ40, respectively.

Figure 11 shows the far-UV CD spectra for the two p3 peptides studied, Aβ17-40 and Aβ17-42. Both peptides show distinct β-sheet structures which is reflected in their deconvoluted spectra shown in Table 1. As expected, Aβ17-42 contains slightly more β-sheet structure (45%) compared to Aβ17-40 (38%) while the content of random coil is more pronounced in Aβ17-40 (36%) compared to Aβ17-42 (30%). The extent of α-helix structure is similar for both peptides (4-6%).

Figure 12 shows the impact of biotinylation on the secondary structures of Aβ40 and Aβ42 upon two weeks of incubation. For Aβ40 biotinylation seems to induce β-sheet formation, especially for the beta-amyloid (1-40)-Lys (biotinoyl) peptide (41% β-sheet instead of 30% for wild type Aβ40). For biotinoyl-beta-amyloid (1-40) the content of β-sheet is 35%. For Aβ42 biotinylation has little effect on the tendency of the peptide to form β-sheets upon

incubation. Biotinylation either way causes a slight decrease in the content of random coil and a small increase in α-helix. This change is smallest for the beta-amyloid (1-42)-Lys-biotinoyl peptide compared to wild type peptide.

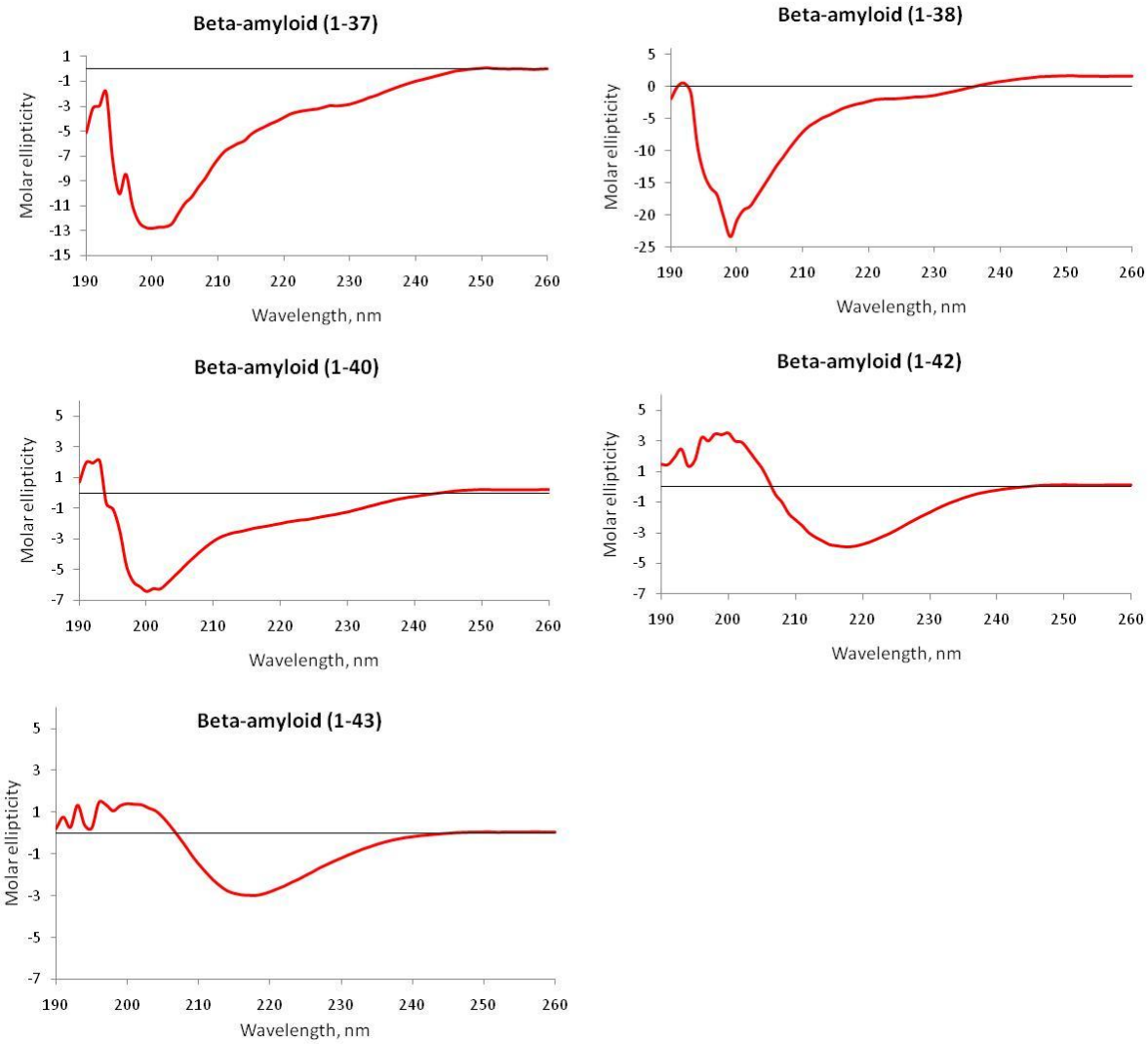

Figure 10 Secondary structure propensities of Aβ peptides varying in length upon 2 weeks of incubation measured by far-UV CD.

Disease-related mutations of Aβ42 all show a tendency to form β-sheet enriched structures similar to wild type Aβ42 (Fig. 13). Overall, there is no strong difference in the far-UV CD spectra upon incubation between wild type Aβ42 and mutated Aβ42, with the following minor exceptions.

- The α-helix contents of E11K (3%) and A21G Aβ42 (3%) are slightly lower compared to wild type Aβ42 (6%).

- D7N (44%) and D23N (44%) Aβ42 show a slightly higher β-sheet content compared to wild type Aβ42 (41%).
- The A21G mutation contains more β-turn (26%) compared to wild type Aβ42 (21%).
- The E11K mutation shows more tendency to random coil structure (35%) compared to wild type Aβ42 (31%).

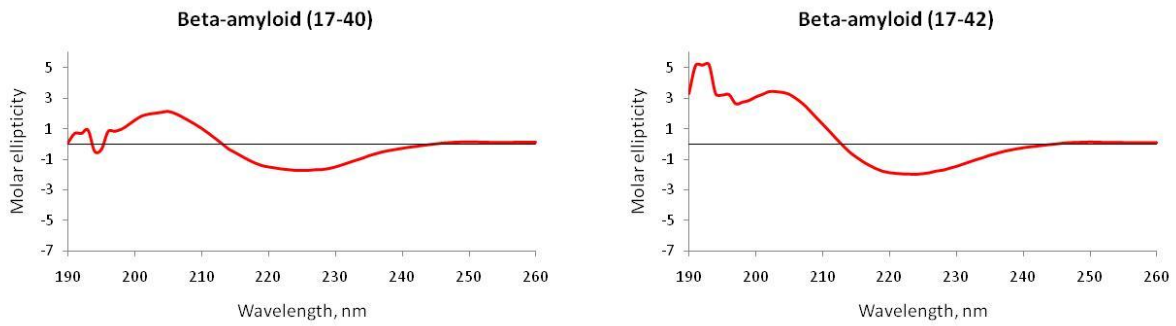

Figure 11 Secondary structure propensities of p3 peptides upon 2 weeks of incubation measured by far-UV CD.

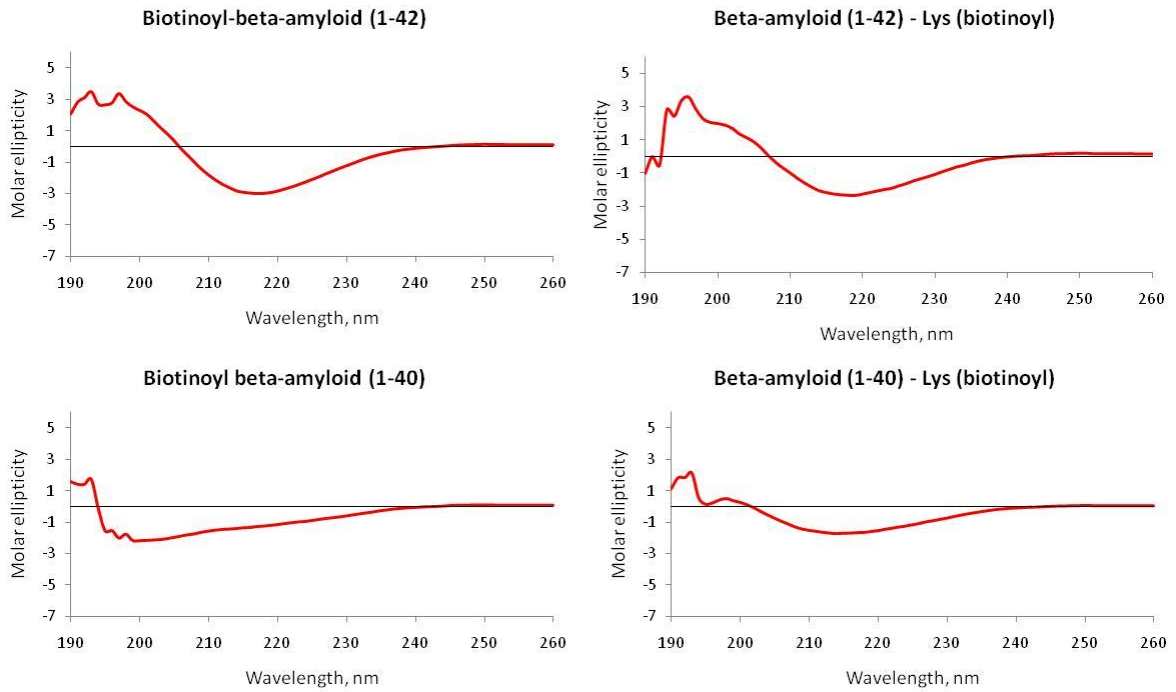

Figure 12 Secondary structure propensities of biotinylated amyloid beta peptides upon 2 weeks of incubation measured by far-UV CD.

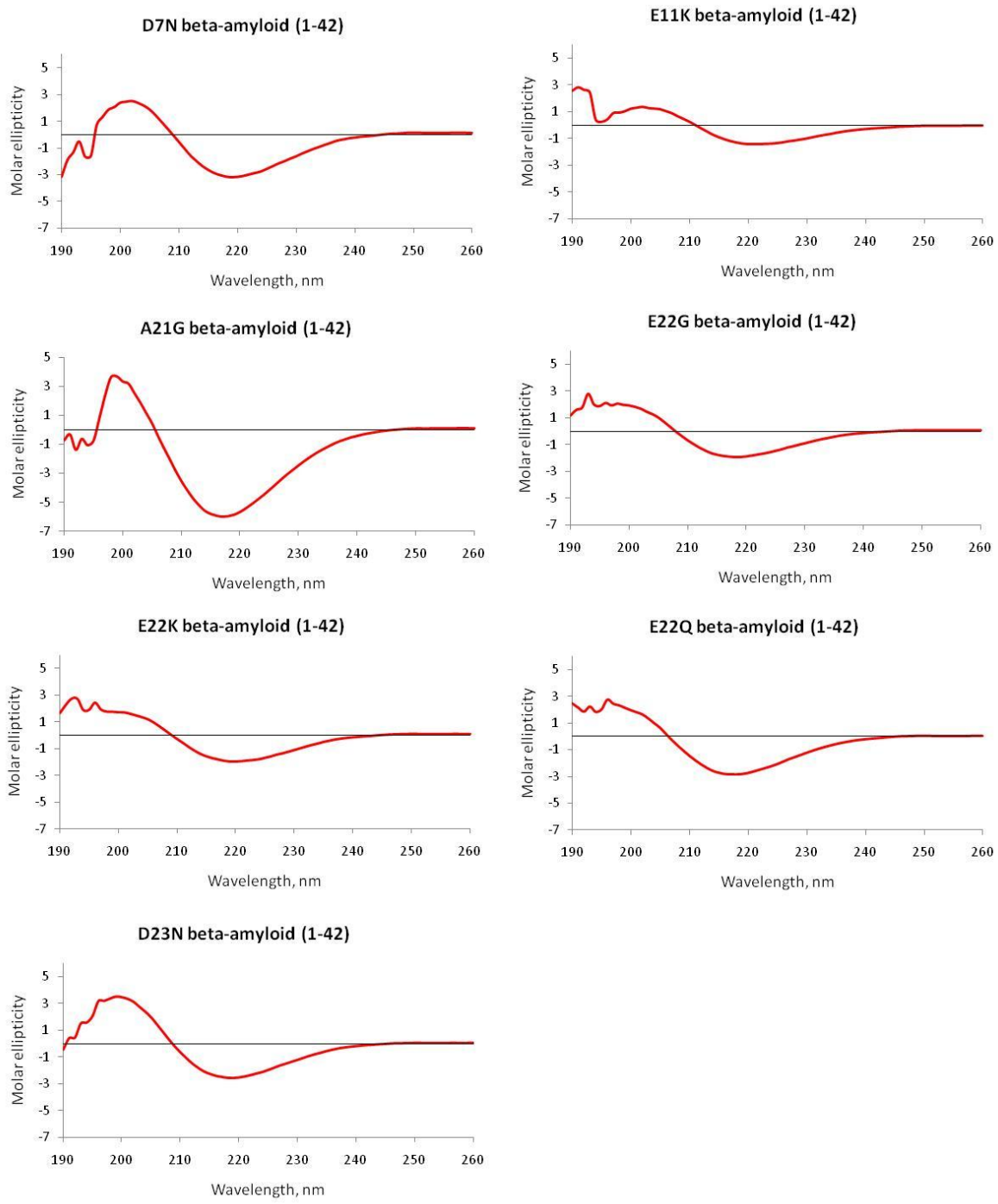

Figure 13 Secondary structure propensities of disease related Aβ42 mutations upon 2 weeks of incubation measured by far-UV CD.

Table 1: Secondary structural components of Aβ-peptides incubated for one week. Analysis has been performed using the Dichroweb website and the CDSSTR algorithm (Lobley et al. 2002, Whitmore and Wallace 2008, Whitmore and Wallace 2004).

Sample	α-helix	β-sheet	β-turn	disordered
Beta-amyloid (1-37)	20	30	24	27
Beta-amyloid (1-38)	15	26	17	42
Beta-amyloid (1-40)	15	30	25	30
Beta-amyloid (1-42)	6	41	21	31
Beta-amyloid (1-43)	5	43	23	31
E11K beta-amyloid (1-42)	3	43	20	35
D7N beta-amyloid (1-42)	7	44	21	28
E22G beta-amyloid (1-42)	6	40	22	32
A21G beta-amyloid (1-42)	3	41	26	32
E22K beta-amyloid (1-42)	5	39	23	31
E22Q beta-amyloid (1-42)	6	41	22	30
D23N beta-amyloid (1-42)	6	44	21	28
Biotinoyl beta-amyloid (1-40)	7	35	23	35
Beta-amyloid (1-40)-Lys (biotinoyl)	7	41	23	29
Biotinoyl beta-amyloid (1-42)	8	44	22	27
Beta-amyloid (1-42)-Lys (biotinoyl)	10	40	23	26
Beta-amyloid (17-40)	6	38	21	36
Beta-amyloid (17-42)	4	45	20	30

Aβ peptide aggregation monitored by Thioflavin T fluorescence

The aggregation rates of all peptides were determined using Thioflavin T (ThT). Early studies demonstrated that *ex vivo* (Naiki et al. 1989) and *ex situ* (Naiki et al. 1990) amyloid fibrils can be detected by ThT, a benzathiole dye. Fibril detection with this dye is based on the observation that binding of ThT to fibrils induces a shift of its excitation and emission maximum from 385 to 450 nm and from 445 to 482 nm, respectively and results in a large enhancement of its fluorescence emission intensity. Hence, ThT is widely used to follow the aggregation kinetics of aggregation processes of a large variety of peptides and proteins, and, used in combination with other methods provides for a convenient and high-throughput technique to detect fibril formation. ThT fluorescence enhancement in the presence of fibrils is thought to be approximately proportional to fibril mass although fibril morphology also determines the accessibility of binding sites for ThT (Naiki et al 1989, Nilsson 2004, Biancalana & Koide 2010).

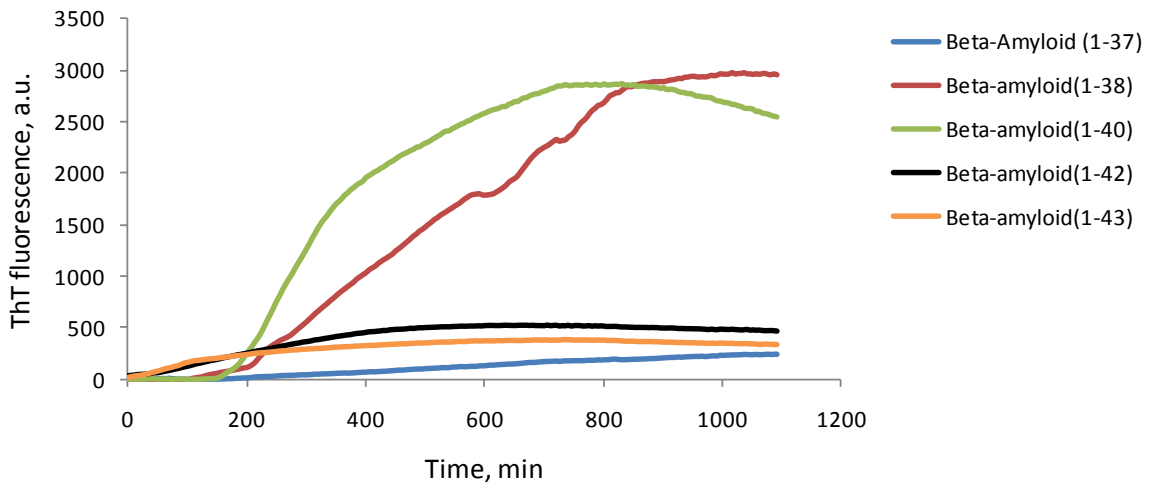

Figure 14 Aggregation rates of Aβ peptides with varying length at a concentration of 1 μM, monitored by ThT fluorescence.

Protein aggregation followed by ThT fluorescence is typically represented by a sigmoidal curve that has been described by a model suggesting nucleation-polymerization kinetics (Harper and Lansbury 1997, Nilsson 2004). The lag phase, during which the fluorescence intensity is minimal, is believed to reflect the formation a thermodynamically stable nucleus. The exponential phase during which the fluorescence intensity rapidly increases is described as the extension of the nucleus to form mature fibrils. The plateau region, during which the fluorescence of ThT no further increases, represents the state of equilibrium between formed aggregates and the monomer and the completion of the fibrillation process. Sometimes fluorescence intensity is found to drop during this period, which indicates the precipitation of ThT-bound aggregates out of the light path detected for fluorescence.

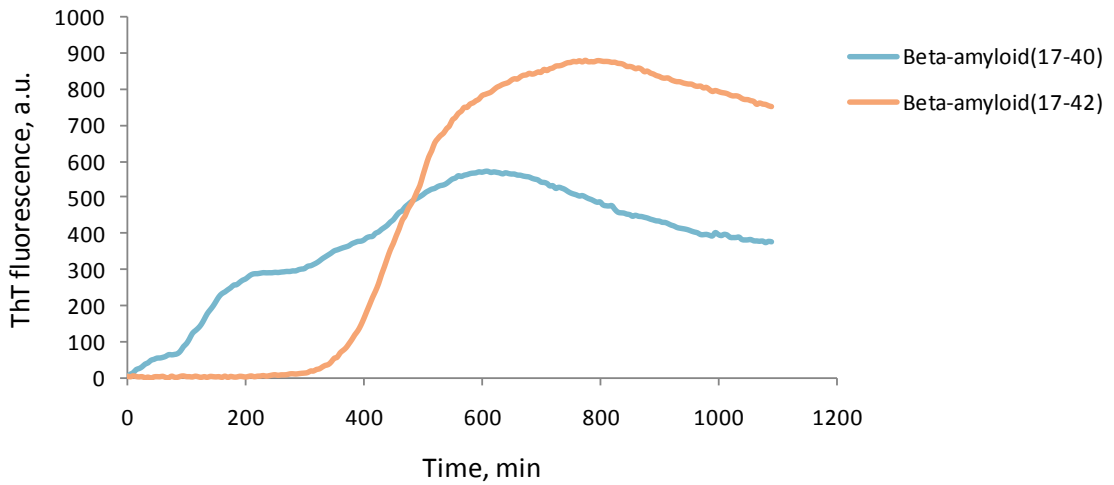

Figure 15 Aggregation rates of p3 peptides at a concentration of 1 μM, monitored by ThT fluorescence.

Figure 14 shows the aggregation kinetics of the Aβ peptides varying in length from 37 to 43 amino acids. Aβ37 (blue) has the lowest aggregation tendency as can be judged from the very low final ThT fluorescence and the late onset of the exponential phase, which is, nonetheless, little pronounced. Aβ38 and Aβ40 show more or less similar aggregation kinetics with a lag phase of ~ 200 min and then increase rapidly to a high fluorescence intensity. A similar profile we reported before for Aβ40 (Kuperstein et al 2010). Both Aβ42 and Aβ43 show very rapid onset of aggregation kinetics, within minutes of starting the experiment. The final fluorescence intensity on the other hand is significantly lower than Aβ38 and Aβ40 which is also consistent with earlier reports (Kuperstein et al 2010, Broersen et al 2011). This is thought to reflect differences in fibril morphology: Aβ38 and Aβ40 form straight negatively stained, twisted fibrils while Aβ42 and Aβ43 form a complex mesh of interconnected aggregates which may not be readily accessible for the ThT probe (Vandersteen, unpublished results).

Figure 15 shows the aggregation kinetics probed by ThT fluorescence of the two p3 peptides Aβ17-40 and Aβ17-42. Aβ17-40 shows a more rapid onset of aggregation than Aβ17-42 (~ 300 min). The final fluorescence of Aβ17-40 is lower than that of Aβ17-42. These results do not reflect the findings for full-length Aβ40 and Aβ42 suggesting that the N-terminal region of Aβ has a regulating function in the aggregation behavior of the peptide.

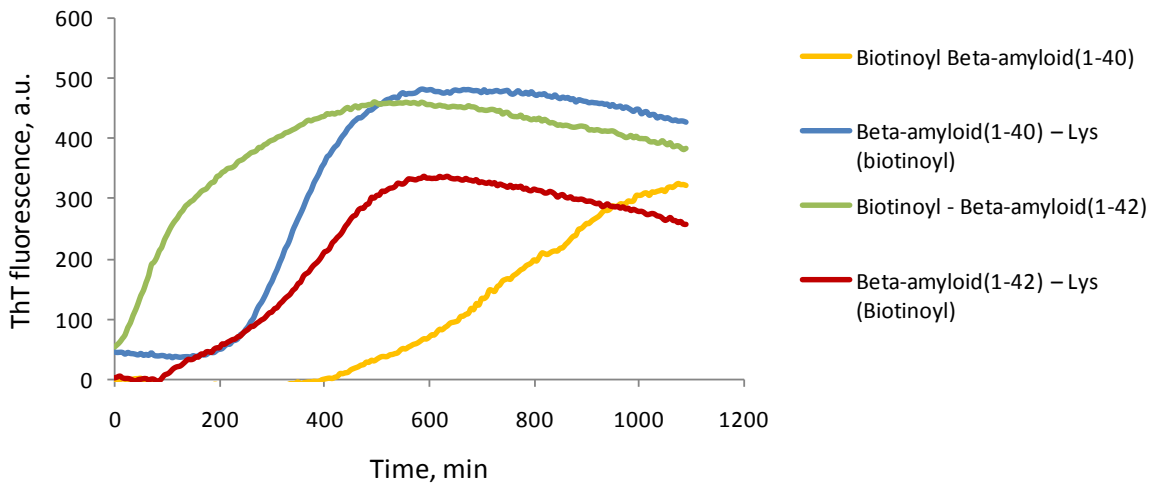

Figure 16 Aggregation rates of biotinylated Aβ peptides at a concentration of 1 μM, monitored by ThT fluorescence.

Figure 16 shows the aggregation rates of biotinylated forms of Aβ40 and Aβ42. The type of biotinylation strongly affects the aggregation kinetics of the peptides. N-terminal biotinylation of Aβ40 increases the lag phase of aggregation to 400 min (unbiotinylated Aβ40 ~200 min, see Fig. 14). The final fluorescence is decreased ~ 10-fold compared to wild type Aβ40. While N-terminal biotinylation of Aβ40 delays the onset of aggregation, the attachment of a C-terminal lysine coupled to the biotinylation group shortens the lag phase to ~ 100 min which is consistent with the predictions obtained with the Tango algorithm (Fig.

6) and far-UV CD spectra which showed extensive β-sheet formation of this form of Aβ40 (Fig. 12).

N-terminal biotinylation does not affect the aggregation profile of Aβ42 much, when compared to wild type Aβ42 (Fig. 14). The attachment of a C-terminal lysine followed by biotinylation delays the aggregation kinetics of Aβ42 compared to N-terminal biotinylation, while the Tango algorithm and far-UV CD show indistinguishable behavior of wild type Aβ42 and the C-terminally biotinylated form.

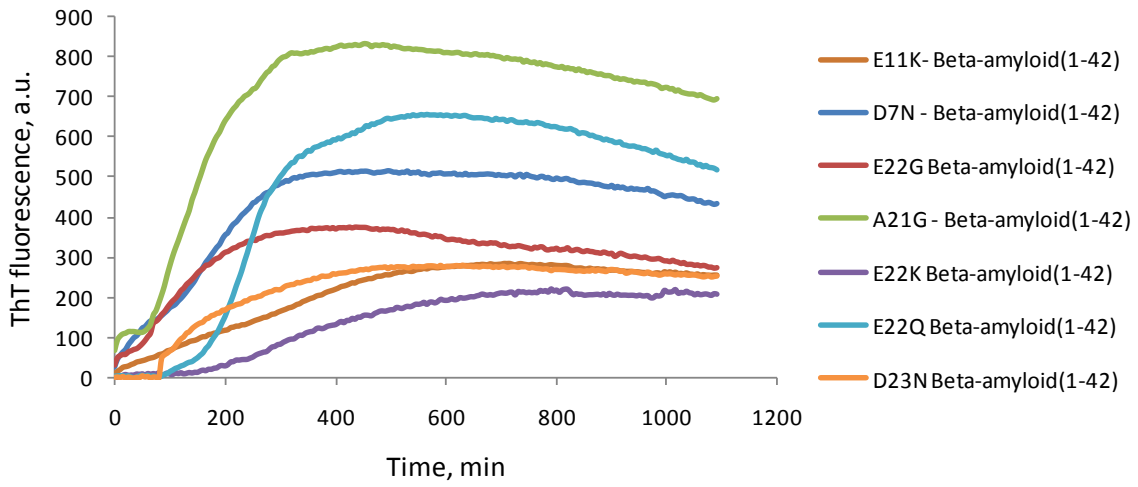

Figure 17 Aggregation rates of disease related mutant Aβ42 peptides at a concentration of 1 μM, monitored by ThT fluorescence.

Aggregation of Aβ42 is affected to various extents by previously identified familial mutations (Fig. 17). Wild type Aβ42 aggregates without a lag phase. All mutated forms of Aβ42 also aggregate without lag phase with the exceptions of E22K Aβ42 (lag phase ~150 min), E22Q Aβ42 (lag phase ~100 min), and D23N Aβ42 (lag phase ~ 80 min). The final fluorescence intensity is generally low for all mutations but is lowest for E22K Aβ42 (200 a.u.), D23N Aβ42 (250 a.u.), E11K Aβ42 (250 a.u.) and E22G Aβ42 (250 a.u.) compared to 500 a.u. for wild type Aβ42. The fluorescence intensity for A21G Aβ42 is highest at 750 a.u. We previously reported minor differences in aggregation kinetics probed by ThT between wild type Aβ42 and the E11K mutation in which the E11K mutation aggregated slightly faster and with a slightly higher final fluorescence intensity compared to wild type Aβ42 (Zhou et al. 2011). These measurements were however performed at a concentration of 25 μM peptide. Aggregation is generally a concentration-dependent process and this relationship can be strongly affected by the type of peptide under investigation. It is thus possible that the concentration dependence of E11K Aβ42 is different compared to wild type Aβ42.

Aβ aggregate morphology investigated by Transmission Electron Microscopy

The morphology of the formed aggregates upon incubation for 2 weeks was investigated using Transmission Electron Microscopy.

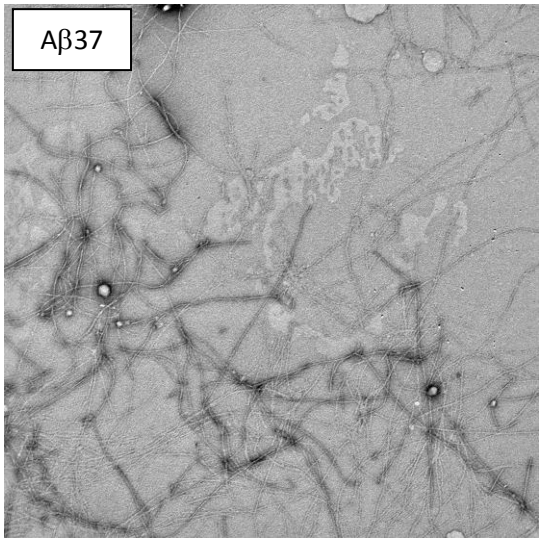

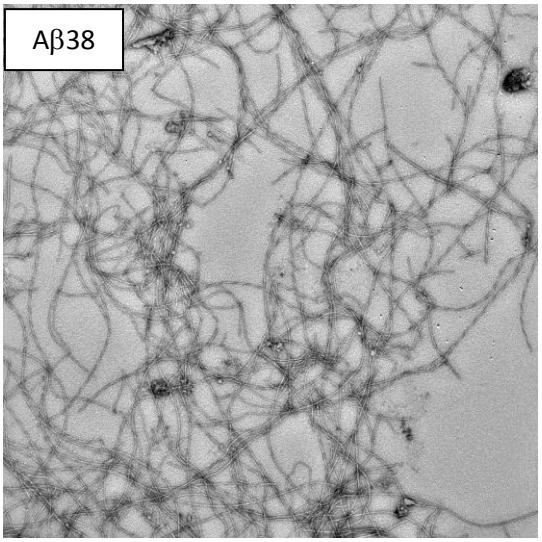

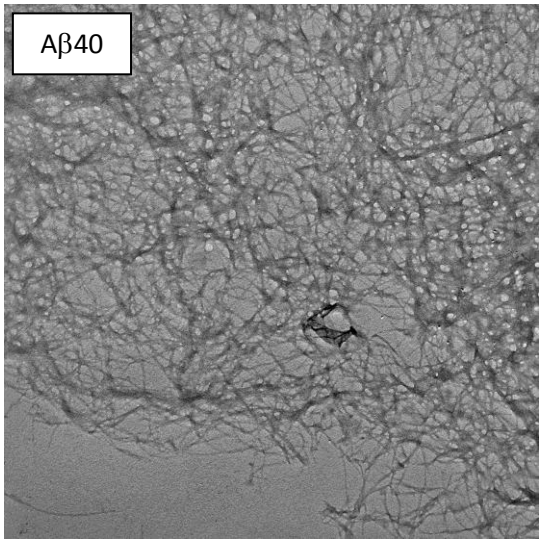

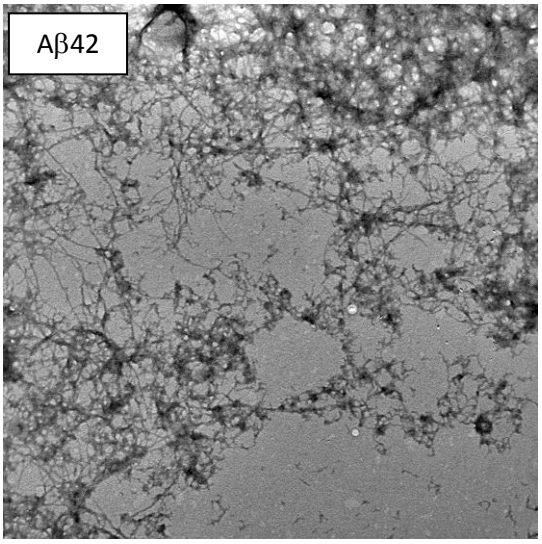

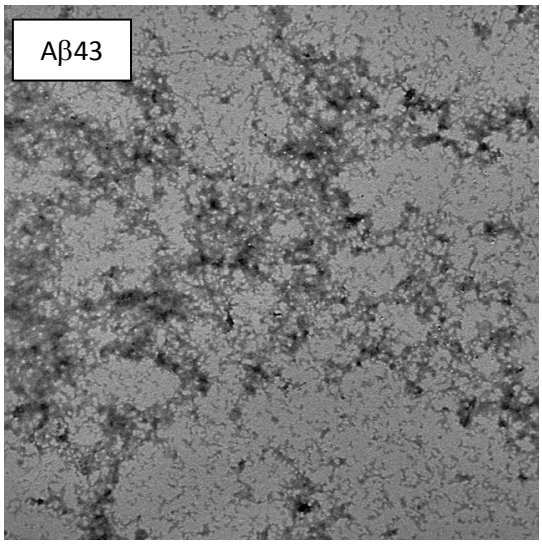

Figure 18 Aggregate morphology of Aβ peptides with varying length. Top left: Aβ37, top right: Aβ38, middle left: Aβ40, middle right: Aβ42, bottom left: Aβ43.

Figure 18 shows the aggregate morphology of Aβ peptides with increasing peptide length. Short Aβ peptides Aβ37 and Aβ38 show predominantly negatively stained well-defined fibrils with a periodic twist. With increasing peptide length the morphology seems to transform from amyloid fibrillar into predominantly amorphous aggregates which interact strongly with the uranyl acetate stain, but little with ThT (Fig. 14). Aβ42 shows a mixture of fibrillar and amorphous aggregates while Aβ43 is exclusively amorphous.

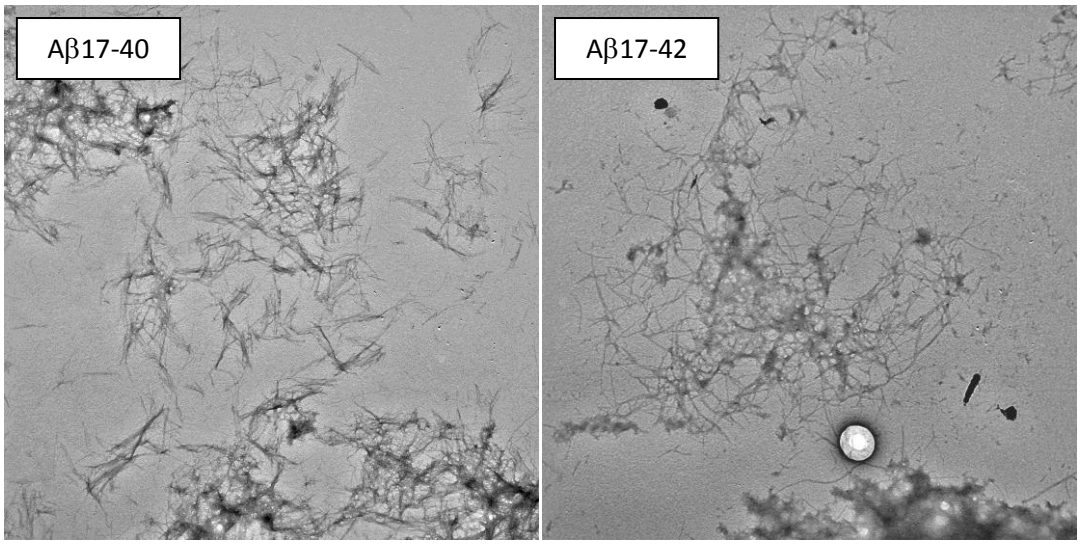

Figure 19 Aggregate morphology of p3 peptides Aβ17-40 (left) and Aβ17-42 (right).

Both p3 peptides form aggregates (Fig. 19) which is consistent with findings using ThT fluorescence (Fig. 15). Aβ17-42 forms a complex mesh of fibrillar material while Aβ17-40 forms laterally associated short fibrils (Fig. 19).

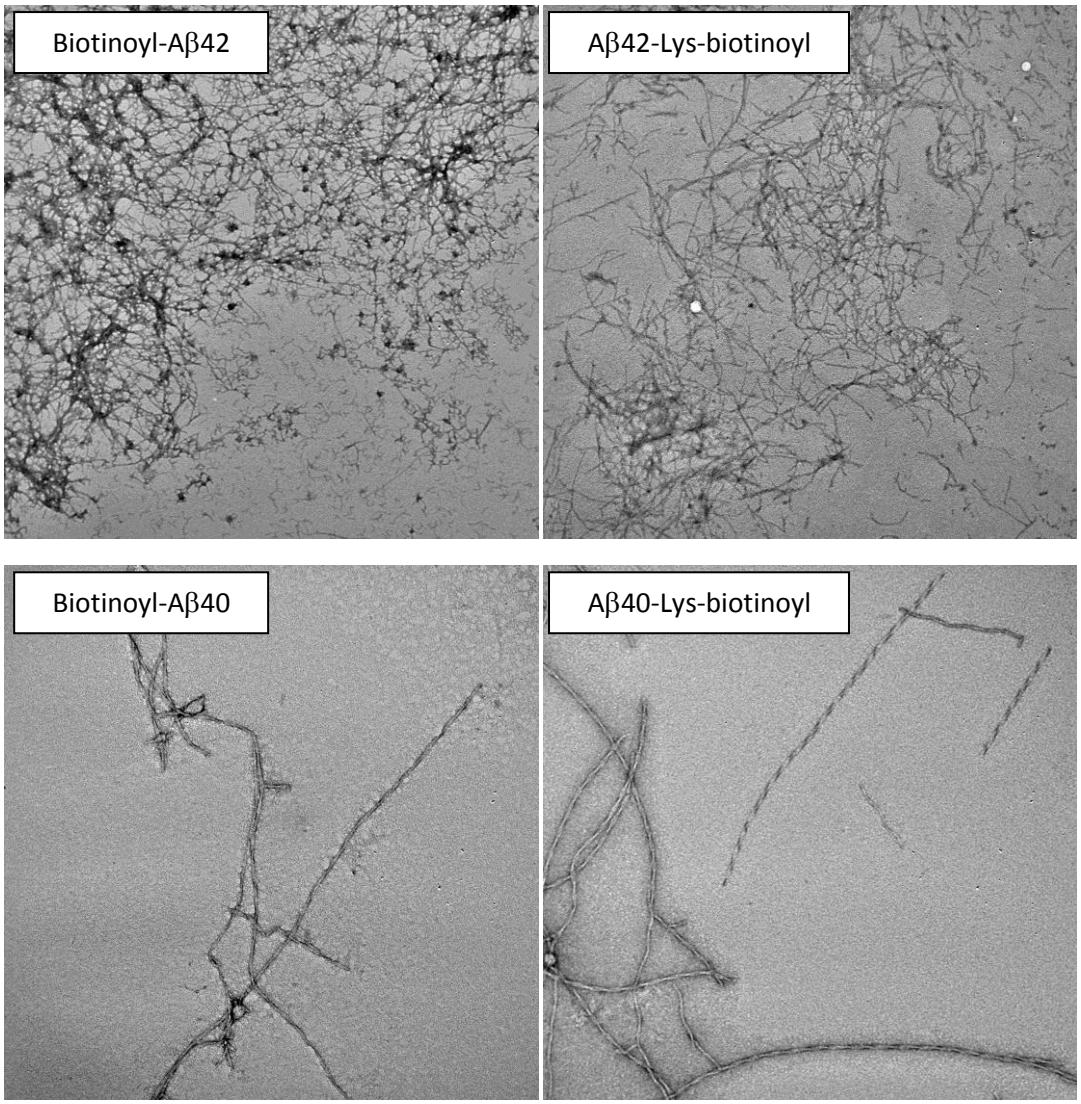

Figure 20 Aggregate morphology of biotinylated Aβ. Top left: biotinoyl-Aβ42, top right: Aβ42-Lys-biotinoyl, bottom left: biotinoyl-Aβ40, bottom right: Aβ40-Lys-biotinoyl.

Biotinylation of Aβ40 and Aβ42 has little effect on the final aggregate morphology: *i.e.* Aβ42 shows a mixture of amorphous and fibrillar aggregates while Aβ40 biotinylation results in long, negatively stained amyloid fibrils containing a periodic twist (Fig. 20).

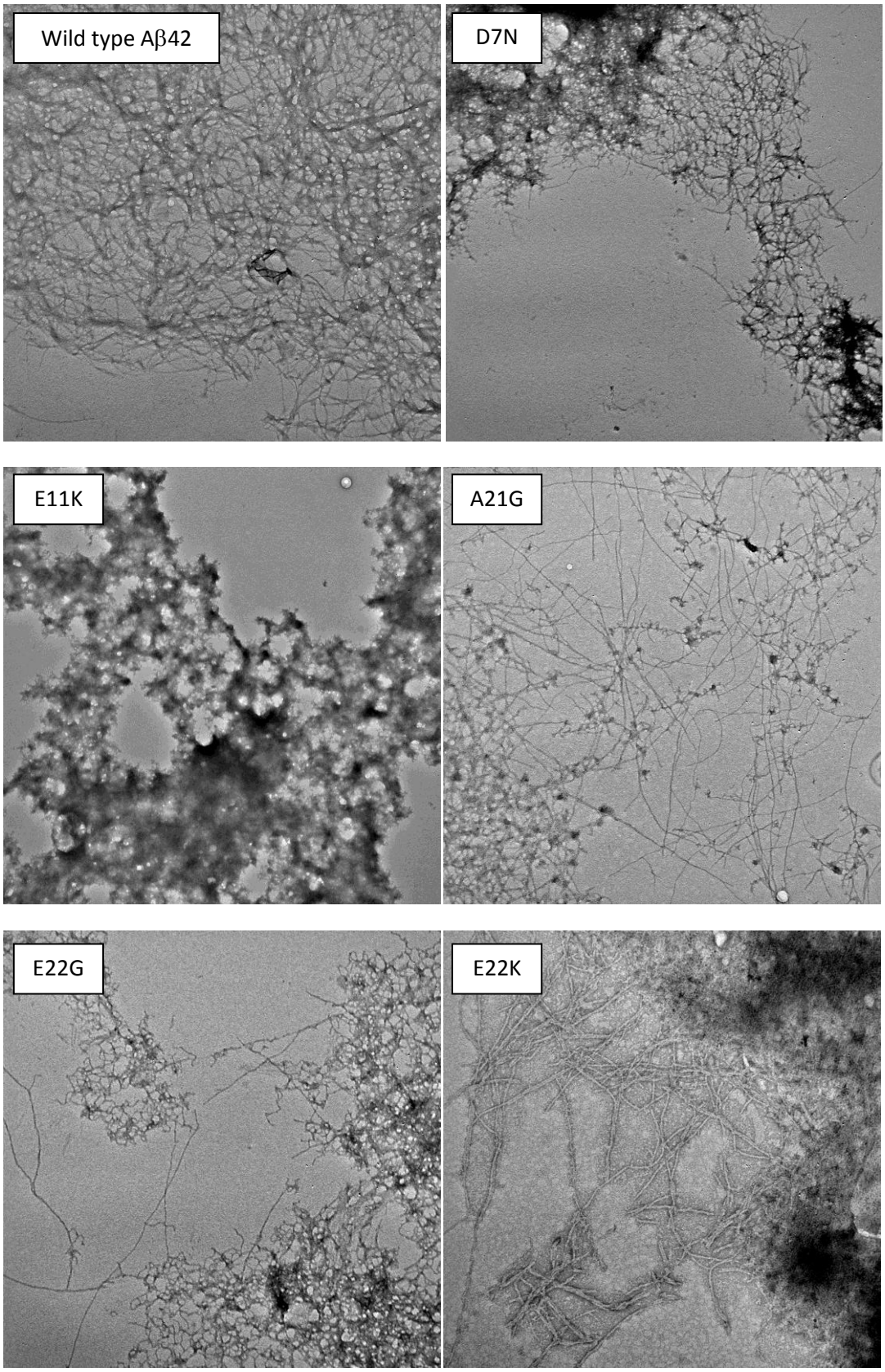
Wild type Aβ42
D7N
E11K
A21G
E22G
E22K

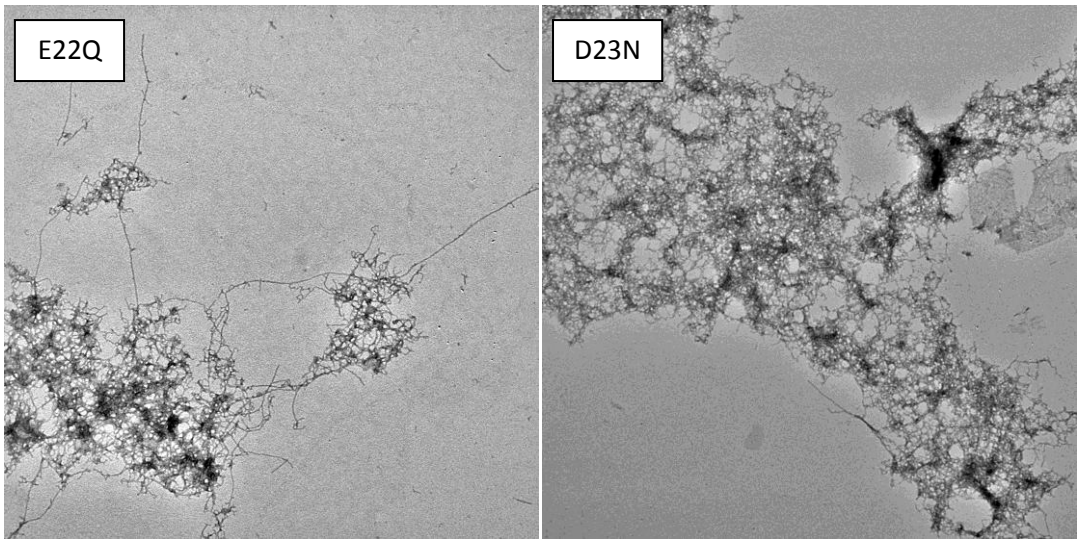

Figure 21 Aggregate morphology of disease-related Aβ mutations. Top row left: wild type Aβ42, top row right: D7N Aβ42, second row left: E11K Aβ42, second row right: A21G Aβ42, third row left: E22G Aβ42, third row right: E22K Aβ42, bottom row left: E22Q Aβ42, bottom row right: D23N Aβ42.

Figure 21 shows the effect of known disease-related mutations of Aβ42 on the aggregate morphology. Mutations that show similar aggregate morphologies compared to wild type Aβ42 include D7N Aβ42, A21G Aβ42, E22G Aβ42 and E22Q Aβ42. A highly amorphous network without any distinguishable individual fibrils is formed for E11K Aβ42 and also a densely aggregated network is observed for D23N Aβ42. Negatively stained fibrils comparable to short Aβ peptides but lacking a visible periodic twist are found for E22K Aβ42.

<u>Oligomeric Aβ assemblies probed by A11 antibody</u>

Immunoblotting of Aβ-containing samples against the A11 antibody developed against oligomeric peptide aids the identification of oligomer-forming peptides (Kayed et al 2003). As oligomers specifically have been identified as the cytotoxic species, this assay provides a biologically relevant qualification of the state of Aβ. The peptide solutions were blotted onto membrane after incubation of 1.5 h, at which time point Aβ42 is commonly highly toxic, and after 2 weeks, when most toxicity of wild type Aβ42 has ceased.

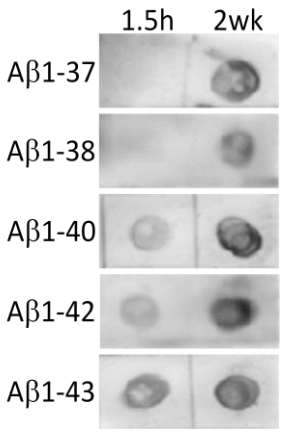

Figure 22 Immunoblot against A11 antibody for different Aβ peptide lengths upon incubation for 1.5 h and 2 weeks.

Figure 22 shows the A11 immunoblot profiles of Aβ37, Aβ38, Aβ40, Aβ42 and Aβ43. After 1.5 h A11 staining increases with increasing Aβ peptide length, suggestive of more oligomer formation when the peptide becomes longer. Both Aβ37 and Aβ38 do not interact with the A11 antibody. Interestingly, after 2 weeks of incubation, all peptides are staining positive for A11 antibody showing that even after 2 weeks of incubation not all oligomeric peptide has converted into an A11-negative fibrillar form.

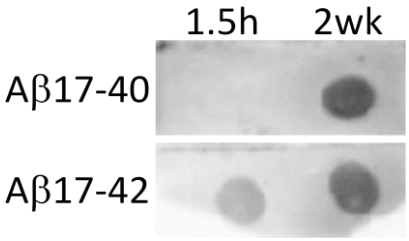

Figure 23 Immunoblot against A11 antibody for different p3 peptide lengths upon incubation for 1.5 h and 2 weeks.

Figure 23 shows that, similar as for full-length Aβ1-40 and Aβ1-42, after 1.5h incubation Aβ17-40 is negative for A11-immunoreactivity while Aβ17-42 stains against the A11 antibody. Also, after 2 weeks of incubation the intensity of staining is strong.

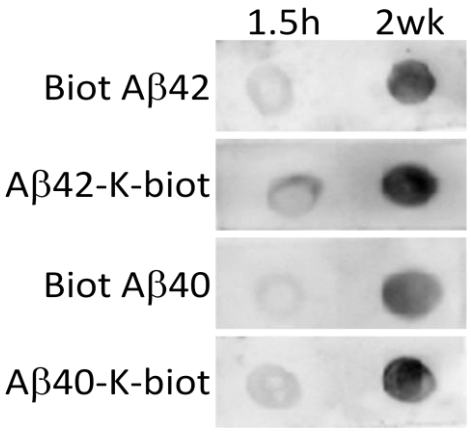

Figure 24 Immunoblot against A11 antibody for biotinylated Aβ40 and Aβ42 upon incubation for 1.5 h and 2 weeks.

Biotinylation of Aβ40 and Aβ42 results in strong anti-A11 intensity after 2 weeks of incubation (Fig. 24) similar to unbiotinylated peptide. All peptides show intensity after 1.5h incubation, although the A11-staining against biotinylated Aβ40 is very weak. Wild type Aβ40 also shows some staining after 1.5 h of incubation (Fig. 22). Biotinylated Aβ42 and Aβ40-Lys-Biotinylated show slightly stronger intensity but still not strong. The reaction of Aβ42-Lys-Biotinylated with A11 antibody is most pronounced but not as intense as after 2 weeks of incubation.

Figure 25 shows the staining patterns of early-onset familial Alzheimer-related mutations of Aβ42 against the A11 antibody. Only the A21G and E22K mutations show a similar pattern as wild type Aβ42, although staining intensity after 2 weeks of incubation is less for E22K Aβ42. The other mutations all show strong staining intensity after 1.5h of incubation, suggestive of accumulation of toxic oligomers at that time point, consistent with the relation of these mutations to early-onset Alzheimer's disease.

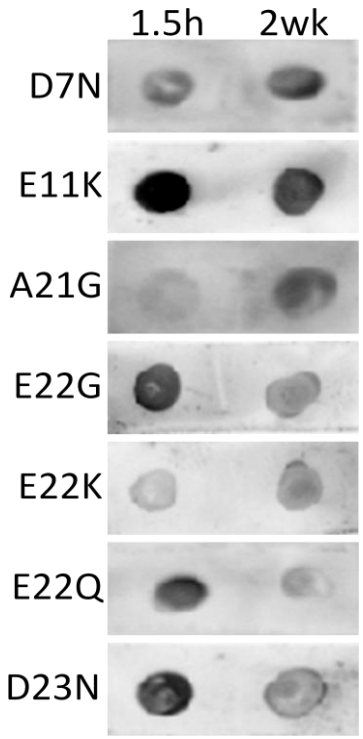

Figure 25 Immunoblot against A11 antibody for Alzheimer-related familial mutations Aβ42 upon incubation for 1.5 h and 2 weeks.

Cytotoxicity of Aβ peptides

The cytotoxic response of Aβ peptides in neuroblastoma SHSY-5Y cells was tested at a final peptide concentration of 5 μM upon incubation for 1.5 h.

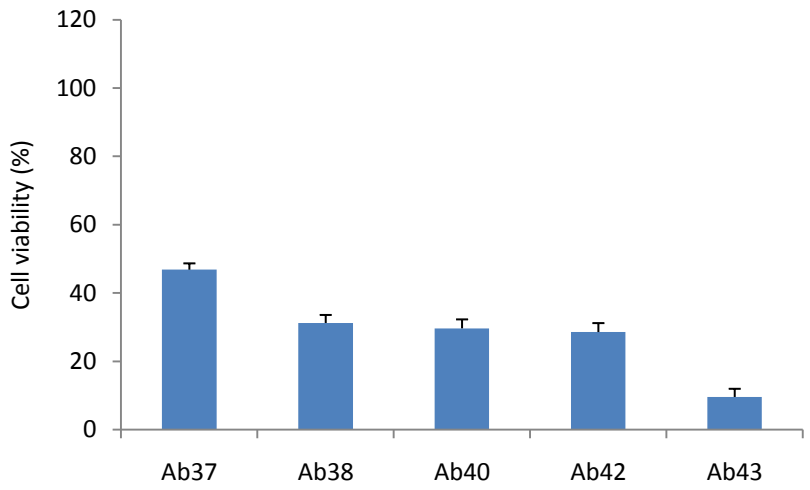

Figure 26 Cytotoxicity response of neuroblastoma cells upon incubation with 5 μM Aβ peptides of varying length.

Increasing Aβ peptide length induces increasing extent of cell death in neuroblastoma cells (Fig. 26). For Aβ42 only ~ 10% of the cells survived the treatment while for Aβ37 ~ 45% of the cells survived, which still is less than half of the viable cells before the treatment with Aβ.

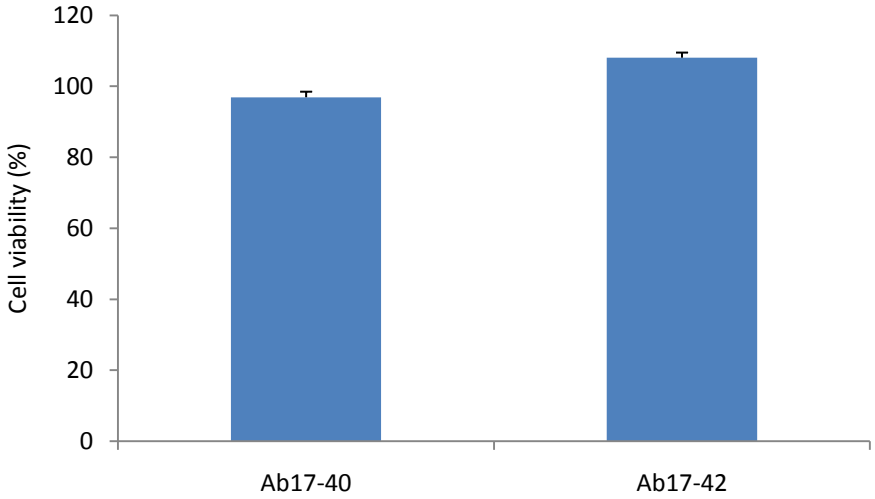

Figure 27 Cytotoxic response of neuroblastoma cells upon incubation with 5 μM p3 peptides.

The two p3 peptides, Aβ17-40 and Aβ17-42, are not toxic at a concentration of 5 μM. For both peptides, ~ 100% of the cells survived the treatment with the peptides (Fig. 27). These findings are consistent with some previous reports which suggested that the p3 fragment is probably non-amyloidogenic but does polymerize into a latticed ultrastructure visible with TEM (Näslund et al 1994) although it has been reported to form a major constituent of Down's syndrome cerebellar amyloid plaques (Lalowski et al 1996). Another report investigating the effects of the p3 peptides on two human neuroblastoma cell lines including SH-SY5Y cells found that treatment of these cells lead to apoptosis through activation of caspase-8 and caspase-3 (Wei et al 2002).

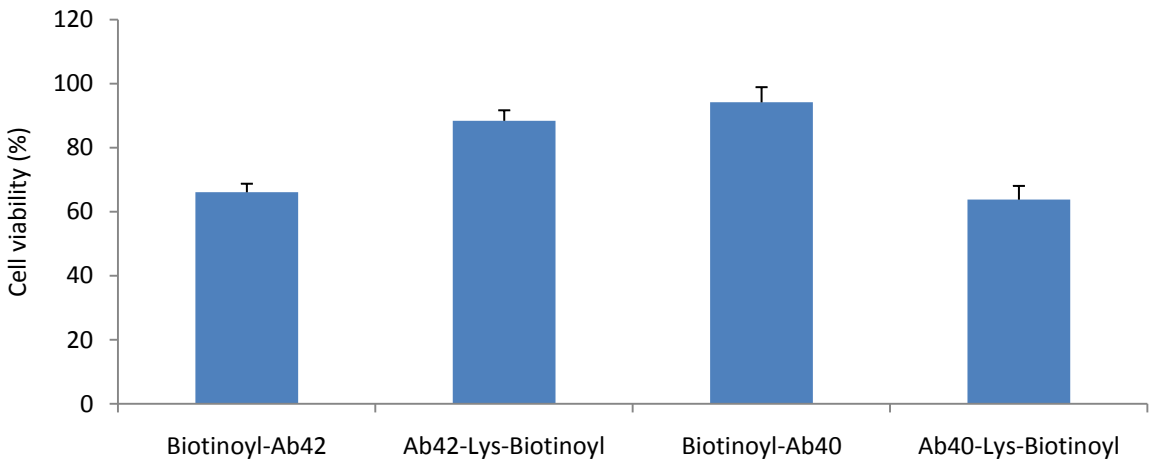

Figure 28 Cytotoxic response of neuroblastoma cells upon incubation with 5 μM biotinylated Aβ40 and Aβ42.

Figure 28 shows that different types of biotinylation of Aβ peptides induce different patterns of cell viability. In both cases, biotinylation appears to at least partially rescue cell toxicity induced by wild type forms of Aβ40 and Aβ42: incubation with wild type Aβ40 results in a cell viability of ~ 30% while incubation with C-terminal biotinylated Aβ40 gave rise to a cell viability of ~ 64% (Fig. 26) and N-terminal biotinylation increases cell viability to ~ 94%. Clearly biotinylation affects the cytotoxic response to the peptide and the type of biotinylation (C- or N-terminal) has a varying impact on cell viability. Aβ42 shows a similar pattern: Incubation of neuroblastoma cells with wild type Aβ42 results in a remaining percentage of viable cells of ~ 29% (Fig. 26). Incubation with N- and C-terminally biotinylated Aβ42 results in cell viabilities of ~ 66% and ~ 88%, respectively.

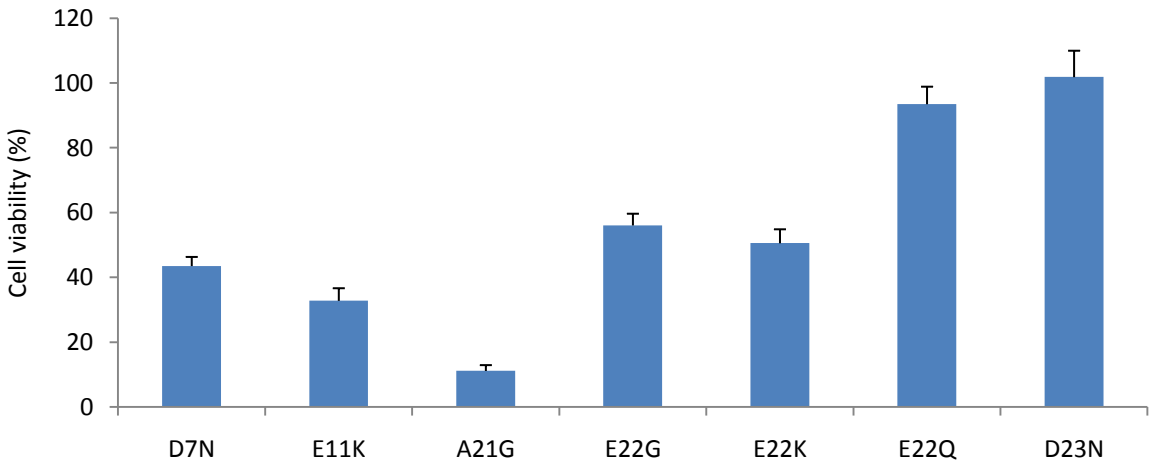

Figure 29 Cytotoxicity of neuroblastoma cells upon incubation of 5 μM Alzheimer's related mutated Aβ peptides.

Figure 29 shows the response of neuroblastoma cells to incubation with Aβ42 carrying various known Alzheimer-related mutations. Wild type Aβ42 results in a percentage of viable cells after incubation of ~ 29% (Fig. 26). The only peptide that is significantly more toxic than wild type Aβ42 is the A21G mutated peptide with a cell survival of only 11% after incubation. E11K and D7N approach wild type cell viability with 33% and 44% cell survival, respectively, followed closely by the E22K and E22Q mutations with cell viabilities of 51% and 56%, respectively. E22Q and D23N are least toxic at 93% and 102% viable cells, respectively.

Concluding remarks

The peptides produced by JPT generally result in sufficient yield upon solubilization and produce fibrillar material similar to ready published images. The peptides preparations are suitable for application in a range of biophysical and cytotoxicity assays and to study in-between variation upon peptide modification in a reproducible manner.

References

Abad-Rodriguez J, Ledesma MD, Craessaerts K, Perga S, Medina M, Delacourte A, Dingwall C, De Strooper B, Dotti CG (2004). Neuronal membrane cholesterol loss enhances amyloid peptide generation. *J Cell Biol* 167: 953-960.

Biancalana M, Koide S (2010). Molecular mechanism of Thioflavin-T binding to amyloid fibrils. *Biochimica et Biophysica Acta* 1804:1405-1412.

Bohrmann B, Tjernberg L, Kuner P, Poli S, Levet-Trafit B, Näslund J, Richards G, Huber W, Döbeli H, Nordstedt C (1999). Endogenous proteins controlling amyloid β-peptide polymerization. *J Biol Chem* 274: 15990-15995.

Broersen, K., Jonckheere, W., Rozenski, J., Vandersteen, A., Pauwels, K., Pastore, A., Rousseau, F., Schymkowitz, J. (2011). A standardized and biocompatible preparation of aggregate-free amyloid beta peptide for biophysical and biological studies of Alzheimer's disease. *Protein Engineering, Design & Selection*. Doi: 10.1093/protein/gzr020.

Brorsson A-C, Bolognesi B, Tartaglia GG, Shammas SL, Favrin G, Watson I, Lomas DA, Chiti F, Vendrusculo M, Dobson CM, Crowther DC, Luheshi LM (2010). Intrinsic determinants of neurotoxic aggregate formation by the amyloid β peptide. *Biophys J* 98: 1677-1684.

Bugiani O, Giaccone G, Rossi G, Mangieri M, Capobianco R, Morbin M, Mazzoleni G, Cupidi C, Marcon G, Giovagnoli A, Bizzi A, Di Fede G, Puoti G, Carella F, Salmaggi A, Romorini A, Patruno GM, Magoni M, Padovani A, Tagliavini F (2010). Hereditary cerebral hemorrhage with amyloidosis associated with the E693K mutation of APP. *Arch Neurol* 67: 987-995.

Fernandez-Escamilla AM, Rousseau F, Schymkowitz J, & Serrano L (2004). Prediction of sequence-dependent and mutational effects on the aggregation of peptides and proteins. *Nature Biotechnology* 22(15361882):1302-1306.

Frost D, Gorman PM, Yip CM, Chakrabartty A (2003). Co-incorporation of A beta 40 and A beta 42 to form mixed pre-fibrillar aggregates. *Eur J Biochem* 270: 654–663.

Grabowski TJ, Cho HS, Vonsattel JP, Rebeck GW, Greenberg SM (2001). Novel amyloid precursor protein mutation in an Iowa family with dementia and severe cerebral amyloid angiopathy. *Ann Neurol* 49: 697-705.

Harper JD, Lansbury Jr PT (1997). Models of amyloid seeding in Alzheimer's disease and scrapie: mechanistic truths and physiological consequences of the time-dependent solubility of amyloid proteins. *Annu Rev Biochem* 66:385-407.

Hendriks L, van Duijn CM, Cras P, Cruts M, van Hul W, van Harskamp F, Warren A, McInnis MG, Antonarakis SE, Martin JJ, Hofman A, Van Broeckhoven C (1992). Presenile dementia and cerebral haemorrhage linked to a mutation at codon 692 of the β-amyloid precursor protein gene. *Nature Gen* 1: 218-221.

Jan A, Gokce O, Luthi-Carter R, Lashuel HA (2008) The ratio of monomeric to aggregated forms of Abeta40 and Abeta42 is an important determinant of amyloid-beta aggregation, fibrillogenesis, and toxicity. *J Biol Chem* 283: 28176–28189.

Kamino K, Orr HT, Payami H, Wijsman EM, Alonso ME, Pulst SM, Anderson L, O'dahl S, Nemens E, White JA, Sadovnick AD, Ball MJ, Kaye J, Warren A, McInnis M, Antonarakis SE, Korenberg JR, Sharma V, Kukull W, Larson E, Heston LL, Martin GM, Bird TD, Schellenberg GD (1992). Linkage and mutational analysis of familial Alzheimer disease kindreds for the APP gene region. *Am J Hum Genet* 51: 998-1014.

Kayed R, Head E, Thompson JL, McIntire TM, Milton SC, Cotman CW, Glabe CG (2003). Common structure of soluble amyloid oligomers implies common mechanism of pathogenesis. *Science* 300: 486-489.

Lalowski M, Golabek A, Lemere CA, Selkoe DJ, Wisniewski HM, Beavis RC, Frangione B, Wisniewski T (1996). The 'nonamyloidogenic' p3 fragment (Amyloid β17-42) is a major constituent of Down's Syndrome cerebellar preamyloid. *J Biol Chem* 271: 33623-33631.

Lewczuk P, Esselmann H, Meyer M, Wollscheid V, Neumann M, Otto M, Maler JM, Rüther E, Kornhuber J, Wiltfang J (2003). The amyloid-beta (Abeta) peptide pattern in cerebrospinal fluid in Alzheimer's disease: evidence of a novel carboxyterminally elongated Abeta peptide. *Rapid Commun Mass Spectrom* 17: 1291-1296.

Leissring MA, Lu A, Condron MM, Teplow DB, Stein RL, Farris W, Selkoe DJ (2003). Kinetics of amyloid β-protein degradation determined by novel fluorescence- and fluorescence polarization-based assays. *J Biol Chem* 278: 37314-37320.

Levy E, Carman MD, Fernandez-Madrid IJ, Power MD, Lieberburg I, van Duinen SG, Bots GT, Luyendijk W, Frangione B (1990). Mutation of the Alzheimer's disease amyloid gene in hereditary cerebral hemorrhage, Dutch type. *Science* 248: 1124-1126.

Liu Y, Walter S, Stagi M., Cherney D, Letiembre M, Schulz-Schaeffer W, Heine H, Penke B, Neumann H, Fassbender K (2005). LPS receptor (CD14): a receptor for phagocytosis of Alzheimer's amyloid peptide. *Brain* 128: 1778-1789.

Lobley A, Whitmore L, Wallace BA (2002). DICHROWEB: an interactive website for the analysis of protein secondary structure from circular dichroism spectra. *Bioinformatics* 18:211-212.

Maddalena AS, Papassotiropoulos A, Gonzalez-Agosti C, Signorell A, Hegi T, Pasch T, Nitsch RM, Hock C (2004). Cerebrospinal fluid profile of amyloid beta peptides in patients with Alzheimer's disease determined by protein biochip technology. *Neurodegener Dis* 1: 231-235.

Maurer-Stroh S*, et al.* (2010). Exploring the sequence determinants of amyloid structure using position-specific scoring matrices. *Nature Methods* (20154676).

Naiki H, Higuchi K, Hosokawa M, Takeda T (1989). Fluorometric determination of amyloid fibrils in vitro using the fluorescent dye, Thioflavine T. *Anal Biochem* 177:244-249.

Naiki H, Higuchi K, Matsushima K, Shimada A, Chen W-H, Hosokawa M, Takeda T (1990). Fluorometric examination of tissue amyloid fibrils in murine senile amyloidosis: use of the fluorescent indicator, Thioflavine T. *Laboratory Investigation* 62:768-773.

Näslund J, Jensen M, Tjernberg LO, Thyberg J, Terenius L, Nordstedt C (1994). The metabolic pathway generating p3, an Aβ peptide fragment, is probably non-amyloidogenic. *Biochem Biophys Res Commun* 204: 780-787.

Nelson TJ, Alkon DL (2007). Protection against β-amyloid-induced apoptosis by peptides interacting with β-amyloid. *J Biol Chem* 282: 31238-31249.

Nilsson MR (2004). Techniques to study amyloid fibril formation in vitro. *Methods* 34:151-160.

Nunan J, Small DH (2000). Regulation of APP cleavage by α-, β- and γ-secretases. *FEBS Lett* 483: 6-10.

Snyder SW, Ladror US, Wade WS, Wang GT, Barrett LW, Matayoshi ED, Huffaker HJ, Krafft GA, Holzman TF (1994). Amyloid-beta aggregation: selective inhibition of aggregation in mixtures of amyloid with different chain lengths. *Biophys J* 67: 1216–1228.

Wakutani Y, Watanabe K, Adachi Y, Wada-Isoe K, Urakami K, Ninomiya H, Saido TC, Hashimoto T, Iwatsubo T, Nakashima K (2004). Novel amyloid precursor protein gene missense mutation (D678N) in probable familial Alzheimer's disease. *J Neurol Neurosurg Psychiatry* 75: 1039-1042.

Wang R, Wang B, He W, Zheng H (2006). Wild-type presenilin 1 protects against Alzheimer's disease mutation-induced amyloid pathology. *J Biol Chem* 29: 29.

Wei W, Norton DD, Wang X, Kusiak JW (2002). Aβ 17-42 in Alzheimer's disease activates JNK and caspase-8 leading to neuronal apoptosis. *Brain* 125: 2036-2043.

Whitmore L, Wallace BA (2008). Protein secondary structure analyses from Circular Dichroism spectroscopy: methods and reference databases. *Biopolymers* 89:392-400.

Whitmore L, Wallace BA (2004). DICHROWEB: an online server for protein secondary structure analyses from circular dichroism spectroscopic data. *Nucleic Acids Research* 32:W668-673.

Wiltfang J, Esselmann H, Bibl M, Smirnov A, Otto M, Paul S, Schmidt B, Klafki HW, Maler M, Dyrks T, Bienert M, Beyermann M, Rüther E, Kornhuber J (2002). Highly conserved

and disease-specific patterns of carboxyterminally truncated Abeta peptides 1-38/38/39 in addition to 1-40/42 in Alzheimer's disease and in patients with chronic neuroinflammation. *J Neurochem* 81: 481-496.

Yan Y, Wang C (2007). Abeta40 protects non-toxic Abeta42 monomer from aggregation. *J Mol Biol* 369: 909–916.

Yoshiike Y, Chui DH, Akagi T, Tanaka N, Takashima A (2003). Specific compositions of amyloid-beta peptides as the determinant of toxic beta-aggregation. *J Biol Chem* 278: 23648–23655.

Younkin SG (1998). The role of A beta 42 in Alzheimer's disease. *J Phys (Paris)* 92 (00075978500027): 289-292.

Zhou L, Brouwers N, Benilova I et al (2011). Amyloid precursor protein mutation E682K at the alternative β-secretase cleavage β'-site increases Aβ generation. *EMBO Mol Med* 3:291-302.